Space Sci Rev (2009) 145: 107–135
DOI 10.1007/s11214-008-9471-8

Electric Fields and Magnetic Fields in the Plasmasphere: A Perspective from CLUSTER and IMAGE

Hiroshi Matsui · John C. Foster · Donald L. Carpenter · Iannis Dandouras · Fabien Darrouzet · Johan De Keyser · Dennis L. Gallagher · Jerry Goldstein · Pamela A. Puhl-Quinn · Claire Vallat

Received: 7 July 2008 / Accepted: 27 October 2008 / Published online: 10 January 2009

Abstract The electric field and magnetic field are basic quantities in the plasmasphere measured since the 1960s. In this review, we first recall conventional wisdom and remaining problems from ground-based whistler measurements. Then we show scientific results from CLUSTER and IMAGE, which are specifically made possible by newly introduced features on these spacecraft, as follows. 1. In situ electric field measurements using artificial elec-

H. Matsui (✉) · P.A. Puhl-Quinn
Space Science Center, Morse Hall, University of New Hampshire (UNH), 39 College Road, Durham, NH 03824, USA
e-mail: hiroshi.matsui@unh.edu

P.A. Puhl-Quinn
e-mail: pamela.puhlquinn@unh.edu

J.C. Foster
Massachusetts Institute of Technology (MIT), Westford, MA, USA
e-mail: jfoster@haystack.mit.edu

D.L. Carpenter
Space Telecommunications and Radioscience Laboratory (STAR), Stanford, CA, USA
e-mail: dlc@nova.stanford.edu

I. Dandouras
Centre d'Etude Spatiale des Rayonnements (CESR), Toulouse, France
e-mail: Iannis.Dandouras@cesr.fr

F. Darrouzet · J. De Keyser
Belgian Institute for Space Aeronomy (BIRA-IASB), Brussels, Belgium

F. Darrouzet
e-mail: Fabien.Darrouzet@oma.be

J. De Keyser
e-mail: Johan.DeKeyser@oma.be

D.L. Gallagher
NASA Marshall Space Flight Center (MSFC), Huntsville, AL, USA
e-mail: dennis.l.gallagher@nasa.gov

tron beams are successfully used to identify electric fields originating from various sources. 2. Global electric fields are derived from sequences of plasmaspheric images, revealing how the inner magnetospheric electric field responds to the southward interplanetary magnetic fields and storms/substorms. 3. Understanding of sub-auroral polarization stream (SAPS) or sub-auroral ion drifts (SAID) are advanced through analysis of a combination of magnetospheric and ionospheric measurements from CLUSTER, IMAGE, and DMSP. 4. Data from multiple spacecraft have been used to estimate magnetic gradients for the first time.

Keywords Plasmasphere · Electric Field · Magnetic Field · CLUSTER · IMAGE

1 Introduction

The electric field and magnetic field are two basic physical quantities in the plasmasphere. The electric field, which may contain both potential and induced components, is related both to large scale motions (usually known as convection) of thermal plasma near the Earth and to the magnetic field through the equation $\boldsymbol{E} = -\boldsymbol{V} \times \boldsymbol{B}$, where $\boldsymbol{E}$ is the electric field, $\boldsymbol{V}$ the convection velocity, and $\boldsymbol{B}$ the magnetic field. Convection is driven by dynamo processes acting in the outer magnetosphere and in the ionosphere. Because of the high mobility of plasma along the magnetic field, and hence the high electrical conductivity along the magnetic field, the motions of the plasma that occur as a result of the dynamo forces (or instabilities) are bulk motions involving tubes of ionization that are aligned with the magnetic field. A feature such as the plasmapause that arises as a result of either the dynamo forces or instabilities thus tends to form along a magnetic shell. These characteristics of electric fields and magnetic fields in the plasmasphere have previously been investigated using ground-based observations of whistler waves and in situ spacecraft (see Lemaire and Gringauz 1998). Recently, new observational capabilities by the CLUSTER and IMAGE spacecraft have provided fresh perspectives on how the plasmasphere is a part of the larger magnetospheric system. The combination of CLUSTER, IMAGE, and ground-based data together with modeling capabilities has provided invaluable complementary viewpoints. This introduction (Sect. 1) is organized into two parts as follows. First the early use of whistler measurements to derive electric fields (during both substorms and quiet periods) is reviewed. Second, the accomplishments of the more recent CLUSTER and IMAGE missions are summarized as a bridge to the rest of the review paper. Following the introduction are sections devoted to specific topics, including understanding gained from electric fields deduced from CLUSTER and IMAGE (Sects. 2 and 3), the modern picture of SAPS/SAID (Sect. 4), calculation of magnetic gradients by multiple CLUSTER spacecraft (Sect. 5). The paper concludes with a summary section that reviews CLUSTER and IMAGE observations in the context the early whistler measurements, and discusses outstanding scientific questions for future study.

1.1 Whistler Measurements to Derive Convection

In the early era of plasmaspheric exploration (the 1960s and 1970s), whistler mode signals provided a powerful means of measuring electric fields within the plasmasphere. Two prin-

J. Goldstein
Southwest Research Institute (SWRI), San Antonio, TX, USA
e-mail: jgoldstein@swri.edu

C. Vallat
European Space Agency (ESA), Villafranca, Spain
e-mail: Claire.Vallat@sciops.esa.int

cipal approaches were used: (i) measurements of the dispersion properties of lightning generated whistlers, and (ii) phase and group path measurements of signals from transmitters.

1.1.1 The Whistler Method of Measuring Cross-L Plasma Drifts

In the early 1960s, it was realized that lightning-triggered whistlers propagate on discrete magnetic-field-aligned paths and that the frequency–time (f–t) properties of a given whistler can be used to estimate the whistler path radius, i.e., the radial coordinate of the equatorial crossing point of the particular whistler path (e.g., Smith 1961; Helliwell 1965, pp. 43–61). The data indicated that a whistler path can retain its identity as a discrete structure (presumably an irregularity representing a few percent density enhancement over the background (e.g., Smith 1961) over periods long compared to the interval between successive excitations by lightning (e.g., Carpenter 1966). Thus it became possible to detect the changes with time of a whistler path radius and therefore determine the cross-L velocity of the path (e.g., Carpenter and Stone 1967; Block and Carpenter 1974). Proceeding on the reasonable assumption that such a path remains an equipotential of the magnetospheric electric field over most of its length from hemisphere to hemisphere (e.g., Gonzales et al. 1980), the path's radial velocity was used as a measure of the bulk motion of the plasma surrounding the duct and hence as a measure of the associated east-west component of the magnetospheric electric field. Thanks to an abundance of whistler activity recorded in 1963 and 1965 near the 75°W meridian in Antarctica, such plasma flow measurements became possible at a time when the substorm phenomenon was first being explored in detail (e.g., Carpenter and Stone 1967; Carpenter et al. 1972).

Initial studies revealed that fast inward drifts in the outer plasmasphere near $L = 4$ began with the expansion phase of a substorm. The corresponding westward component of the electric field was inferred to peak in the range ~0.5–1 mV m^{-1}. In cases of temporally isolated substorms, the azimuthal component of the electric field was found to change direction, such that cross-L outward flow began as ground magnetometers showed an end to the substorm-associated field aligned currents (Carpenter and Seely 1976). The intensity and duration of the outward flow were such that the plasmasphere, although subject to distortions in shape imposed by the changes in flow direction, did not appear to change substantially in overall size. However, when substorm activity was prolonged, as in the case of several weak magnetic storms that were studied, the return outward flows were not observed and the global size of the plasmasphere, as seen from a single ground station, was found to shrink substantially (Carpenter et al. 1979).

Abundant Antarctic whistler activity on magnetically quiet days made possible tracking of whistler ducts over extended time periods. Figure 1 shows two case studies: (a) from Siple, Antarctica ($L \approx 4.2$) on 7 July 1973, and (b) from Eights, Antarctica ($L \approx 3.9$) on 13 June 1965 (Carpenter and Seely 1976). The figure is plotted in coordinates of L^{-2} versus time, so that the east-west electric field inferred from a series of data points is approximately proportional to the rate of change of observed L^{-2} with time, regardless of the absolute values of L. The data slopes were similar over paths distributed in L value, attesting to the large scale nature of the plasma motions involved. The most clearly identified features in Fig. 1 are pre-noon outward drifts and post-noon inward motions, which were interpreted as evidence of ionospheric dynamo effects (the SQ, solar-quiet-time, geomagnetic daily variation field, current system).

Figure 2 shows 30-minute averages of whistler-path radial drifts in the plasmasphere at $L \approx 4$ during periods of substorm activity (Carpenter et al. 1979). In spite of limitations imposed by the averaging methods used, several features stand out. There was a rather abrupt

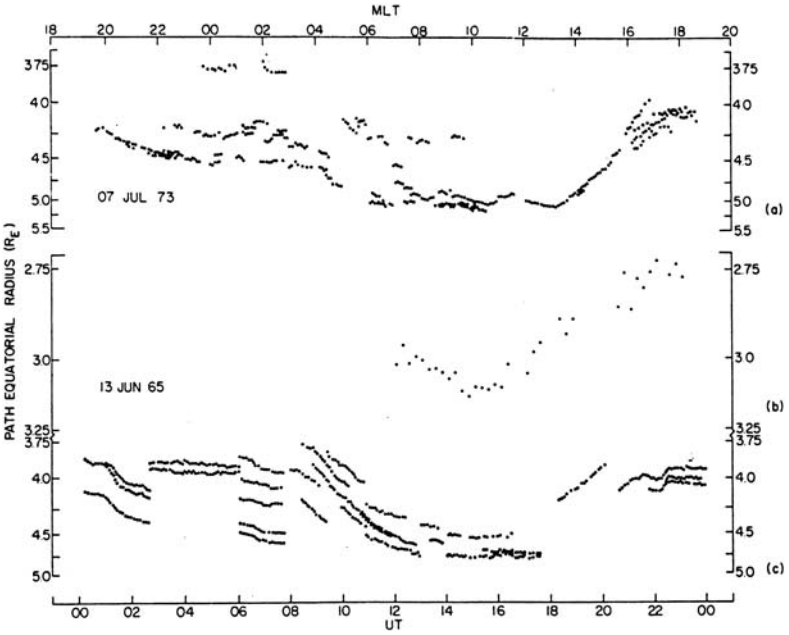

Fig. 1 Whistler path radii time series from two magnetically quiet 24 hour periods showing a strong morning outflow and post-noon inflow, effects that are attributed to an ionospheric dynamo process (the SQ, solar-quiet-time, geomagnetic daily variation field, current system). (Adapted from Carpenter and Seely 1976)

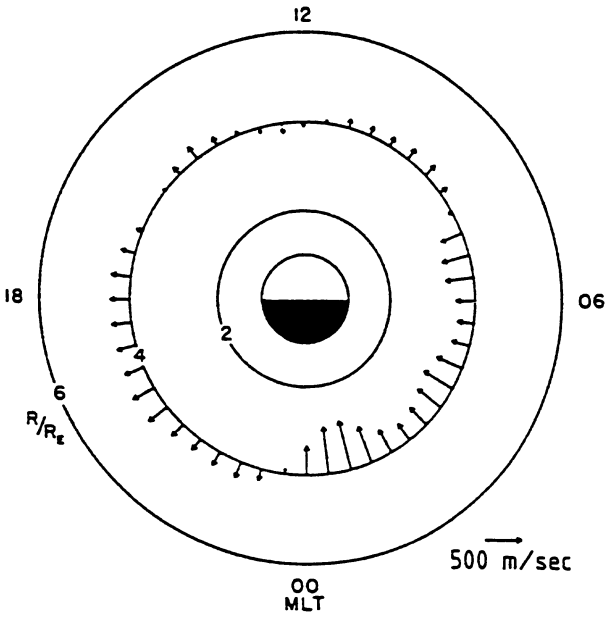

Fig. 2 Average westward electric field in the outer plasmasphere at $L = 4$ during periods of prolonged substorm activity, represented in terms of cross-L flow velocities in the equatorial plane. (Adapted from Carpenter et al. 1979)

transition near midnight from weak outward flow to fast inward flow that persisted into the dawn sector. Moderate outward drifts were observed in the pre-noon sector, followed near noon by weak flows and then later by outward drifts that increased in amplitude near dusk.

1.1.2 Whistler Estimates of the E_y Electric Field Component Near Dusk

Early whistler data did not show evidence of the type of dusk-side stagnation point in plasma flow envisioned in theoretical models that combined a uniform dawn–dusk convection field with a corotation field (Carpenter 1966, 1970). Instead, there were indications of decoupling of the main plasmasphere from the so-called bulge region of larger plasmasphere radius. That is, there was a fairly rapid spatial transition in the generally radial direction from a region dominated by the Earth's rotation to one strongly dominated by the convection electric field. This outer region (very possibly reflecting the effects of what is now called the SAPS electric field; see Sect. 4) regularly exhibited an abrupt westward edge, which was found by the corotating whistler station to be displaced to earlier (afternoon) or later (post-dusk) local times (LT) as magnetic activity increased or decreased, respectively. Using $L \approx 4.5$ as typical of the outer region, the electric field in the dawn dusk direction (E_y component) was estimated to be $\sim$1–4 mV m^{-1} during substorms (as seen from the rotating Earth), about 4 times larger than corresponding (essentially westward) values observed in the post-midnight sector using the whistler drift method (Carpenter 1970).

1.1.3 Measurements on Whistler-Mode Transmitter Signals

Phase and group path measurements on transmitter signals began in New Zealand in the late 1960s when it was found to be possible to measure the Doppler shift on signals at 18.6 kHz from the NLK transmitter in Seattle, Washington (McNeill 1967). The Doppler shift was recognized to be a function both of path drift as well as of changes in the path-integrated electron content, and measurements were later performed that allowed separate estimates of the two effects (e.g., Thomson 1976). Successive redesigns of receivers and refinement of methods led to the possibility of identifying the multiple group delays of minimum shift keying (MSK) signals propagating on a set of magnetospheric paths distributed near $L = 2.5$ while also measuring Doppler shifts on the signals (e.g., Thomson 1981). Observations of two transmitter signals simultaneously, namely NSS (21.4 kHz) and NAA (24.0 kHz) at Faraday (Antarctica), made it possible to separately determine for each observed whistler-mode path the L value (determined from small differences in group delay between the two transmitter signals), cross-L drift velocity, and electron coupling flux (Smith et al. 1987). Figure 3 shows the variation with LT of the average westward electric field at $L \approx 2.5$ for nine quiet days in July 1986 (Saxton and Smith 1989). As in the case of the quiet day whistler data of Fig. 1, the field is eastward in the late morning sector and westward in the afternoon.

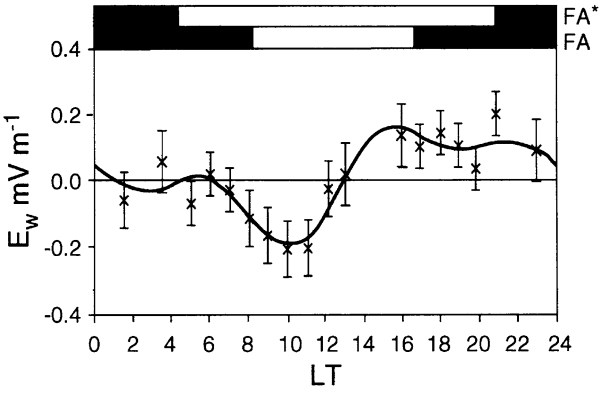

Fig. 3 The variation with local time of the average westward electric field at $L = 2.5$ for nine quiet days in July 1986, obtained from NAA and NSS whistler-mode observations at Faraday, Antarctica. The white sections above indicate the hours of sunlight for Faraday and its conjugate. (Adapted from Saxton and Smith 1989)

Also in agreement with the whistler work, the quiet day field magnitudes remained below $\sim$0.2 mV m^{-1}. Application of this method at the time of a severe magnetic storm on 11–12 September 1986 indicated that the westward electric field at $L \approx 2.5$ near midnight exceeded 1 mV m^{-1} during a period when K_p reached a maximum of 9 (Balmforth et al. 1994).

1.2 CLUSTER and IMAGE Achievements

The CLUSTER and IMAGE spacecraft were both launched in 2000 with new capabilities (respectively, multi-point and imaging observations) that did not exist in previous missions (Escoubet et al. 1997; Burch 2000; De Keyser et al. 2008, this issue). These new capabilities permitted a deeper investigation of the phenomena discovered by ground whistler measurements. Using four identical spacecraft, CLUSTER performs multi-point in situ measurements with high temporal and spatial resolution, making it possible to derive the electric current by calculating the curl of the magnetic field measured by the FluxGate Magnetometer (FGM) (Balogh et al. 2001). Three of CLUSTER's instruments offer electric field information: the Electron Drift Instrument (EDI) (Paschmann et al. 2001), the Electric Field and Wave (EFW) instrument (Gustafsson et al. 2001), and the Cluster Ion Spectrometry (CIS) instrument (Rème et al. 2001). The IMAGE spacecraft was the first to routinely observe global plasmaspheric behavior, providing a new means of diagnosing the global convection field. The Extreme UltraViolet (EUV) imager (Sandel et al. 2001) was designed to measure 30.4 nm sunlight that is resonantly scattered by the He^+ ions that are an important constituent of plasmaspheric material. Because the relatively cold (1 eV) ions of the plasmasphere are primarily influenced by the electric field (via $E \times B$ drift), observation of the time evolution of plasmaspheric structures such as the plasmapause allows derivation of electric fields. The combination of IMAGE data with that of other spacecraft and ground-based observatories has yielded much new insight.

Together, CLUSTER and IMAGE have substantially increased our knowledge and understanding of both plasmaspheric dynamics and the inner magnetospheric electric field that controls them. Early studies recognized that the interplanetary electric field (generated by the motion of the solar wind past the magnetosphere) drives magnetospheric convection, and that the shape of the plasmasphere is roughly determined by the superposition of the electric fields caused by this convection and by the corotation with the Earth (Nishida 1966; Brice 1967). The convection electric field is not only affected by the immediate interplanetary condition but also by the substorm/storm phases, whose relationship with the interplanetary variation is complicated, especially by the fact that currents and fields generated inside the magnetosphere–ionosphere system can modify substantially the convection generated by the solar-wind–magnetosphere interaction. Thus, quantitative understanding of the relationship between the plasmasphere response and interplanetary (solar wind) parameters remains a major puzzle to be solved. The CLUSTER and IMAGE missions have made it possible to compare plasmaspheric measurements with interplanetary monitors such as ACE and WIND and with geomagnetic indices such as *Dst*, K_p, and *AE*, to make progress in the solution to this puzzle.

The mapping of plasmaspheric quantities between high altitude in the magnetosphere and low altitude in the ionosphere emphasizes the important role played by magnetosphere–ionosphere (M–I) coupling in shaping the plasmasphere boundary layer, or PBL (Carpenter and Lemaire 2004). This is also manifested by inter-comparison of data from multiple spacecraft. The new perception of the outer reaches of the plasmasphere as a boundary layer recognizes the unique and important processes found there. The redistribution of plasmaspheric material throughout the coupled magnetosphere–ionosphere system traces out

the convection streamlines and the electric fields associated with a variety of sources and drivers. Features and mechanisms seen for the first time by CLUSTER, IMAGE, and ground-based measurements exhibit a scale size and repeatability, which indicate their fundamental role in the overall system.

In this review, we mainly discuss the following topics.

- The electric field is successfully measured by EDI onboard CLUSTER in the range $L = 4$–10. Electric fields with various origins are identified: solar wind–magnetosphere interaction, M–I coupling including SAPS, ionospheric dynamo, and ultra low frequency (ULF) waves. The solar wind–magnetosphere interaction is statistically examined in terms of correlation between the Z component of the interplanetary magnetic field (IMF) and inner magnetospheric electric fields. The investigation on IMF B_Y dependence reveals the importance of M–I coupling in addition to the solar wind–magnetosphere interaction (Sect. 2).
- Electric fields and flows deduced from sequences of plasmasphere images have provided information about the timing and global phenomenology of erosion during storms and substorms. IMAGE data have been used to study electric fields that arise from ionospheric closure of the partial ring current, including shielding and SAPS, providing quantitative global measurements that have furthered our knowledge of the inner magnetospheric electric field, and helped improve electric field models (Sect. 3).
- SAPS or SAID are examined by multiple spacecraft analysis. IMAGE data show plasmaspheric plumes, which are adjacent to the SAPS channel measured by DMSP. Comparison between magnetically conjugate CLUSTER and DMSP electric field data shows the absence of significant field-aligned potential drops between the two spacecraft, while the field-aligned current comparison suggests partial perpendicular closure between the spacecraft (Sect. 4).
- The CLUSTER mission provides the opportunity to study the plasmasphere with four-point measurements, permitting examination of the geometry and orientation of the overall magnetic field in the plasmasphere. A detailed analysis of a typical CLUSTER pass through the plasmasphere is presented, in which the direction of the gradient is compared with the local field vector. Particular attention is paid to the relative roles of the gradient components along and transverse to magnetic field lines (Sect. 5).

2 Inner Magnetospheric Electric Fields Measured by CLUSTER

Because of their profound influence on the dynamics of particle populations (and particularly upon the cold dense particles of the plasmasphere), measuring or deriving inner magnetospheric electric fields remains an active area of research. Electric fields have been determined indirectly by the shape of the plasmapause (e.g., Maynard and Chen 1975) and the location of the inner edge of the plasmasheet (McIlwain 1974), while ground-based measurements are common tools to determine the electric fields (e.g., Carpenter and Seely 1976; Wand and Evans 1981; Foster et al. 1986). Direct in situ measurements have also been provided by the double probe technique (Maynard et al. 1983; Rowland and Wygant 1998) and by the electron drift technique (Baumjohann et al. 1985; Quinn et al. 1999). EDI onboard CLUSTER measures in situ magnetospheric electric fields with high quality and with good data coverage comparable to or better than these previous measurements, which makes it possible to perform comprehensive studies on the inner magnetospheric electric fields.

2.1 EDI Onboard CLUSTER

EDI measures electric fields at the in situ spacecraft location (Paschmann et al. 2001). Electron beams with an energy of 1 keV (and 500 eV for a small number of cases) are emitted from two pairs of guns in the direction perpendicular to the ambient magnetic field. Electron beams subsequently experience cyclotron motion and drift motion, and fractions of the beams return to two pairs of detectors. Drift motions include both $\boldsymbol{E} \times \boldsymbol{B}$ and ∇B components, although the latter contribution is much smaller at the above beam energies in the inner magnetosphere. CLUSTER EDI actually measures drift step length during approximately one or multiple gyroperiods by triangulation and/or time-of-flight methods. Here we try to determine two perpendicular components of the electric field from this drift step length.

The EDI tends to work well in the inner magnetosphere, for the following reasons. First, owing to the relatively large magnetic field strength the gyroperiod of electrons in the beam is small, minimizing the parallel (along the magnetic field) dispersion of beams returning to the detectors. Second, inside the plasmasphere there are few natural plasma sheet electrons to contaminate or mask the instrument beams (Quinn et al. 2001). (Note that the EDI instrument data also includes an estimate of the ambient or "background" electrons.) EDI performance suffers in inner magnetospheric regions with significant natural electron fluxes, and during geomagnetically active periods (such as substorms and storms) during which highly variable electric fields make tracking of the electron beams by the onboard controller more difficult. Therefore, electric field data are often not available in these regions/periods. Otherwise, the electric fields are usually measured successfully by EDI. These data are relatively reliable compared to those from the other instruments (Eriksson et al. 2006; Puhl-Quinn et al. 2008). These electric field data have been analyzed by Matsui et al. (2003, 2004, 2005) and by Puhl-Quinn et al. (2007).

The optimal time resolution of the CLUSTER EDI data is 1 second. There are occasional data gaps caused by electron beam tracking difficulties (as noted above). The CLUSTER spacecraft were originally deployed with perigees at 4 R_E and apogees at 20 R_E on polar orbits with a period of 57 hours. Analysis of CLUSTER EDI data from this earlier period has been performed for $4 < L < 10$. Modification of CLUSTER's orbits since 2006 has resulted in a lower perigee, in principle making it possible to study of electric field for $L < 4$, though extension to lower L is beyond the scope of this review. CLUSTER's pre-2006 orbits covered all magnetic local times (MLT) once per year owing to annual precession as the Earth revolves around the Sun. The CLUSTER spacecraft were launched in summer 2000, and have made available a wealth of data to perform both statistical and case studies. Data from C1 and C3 are available continuously. Data from C2 are available until April 2004, while EDI is not operated on C4. In the work reviewed here the data chosen for analyses have been identified to be of good quality by the ground software.

2.2 Inner Magnetospheric Electric Fields

2.2.1 Case Studies

Matsui et al. (2003) reported electric field observations on 13 April 2002 made by EDI onboard CLUSTER (Fig. 4). The horizontal axis shows the magnetic latitudes (MLAT) between -60 and $+60°$. The results from C1, C2, and C3 are shown by black, red, and green colors, respectively. The three spacecraft measure fairly similar features indicating spatial variation is small compared to the distance between spacecraft examined here (∼90–160 km). Radial

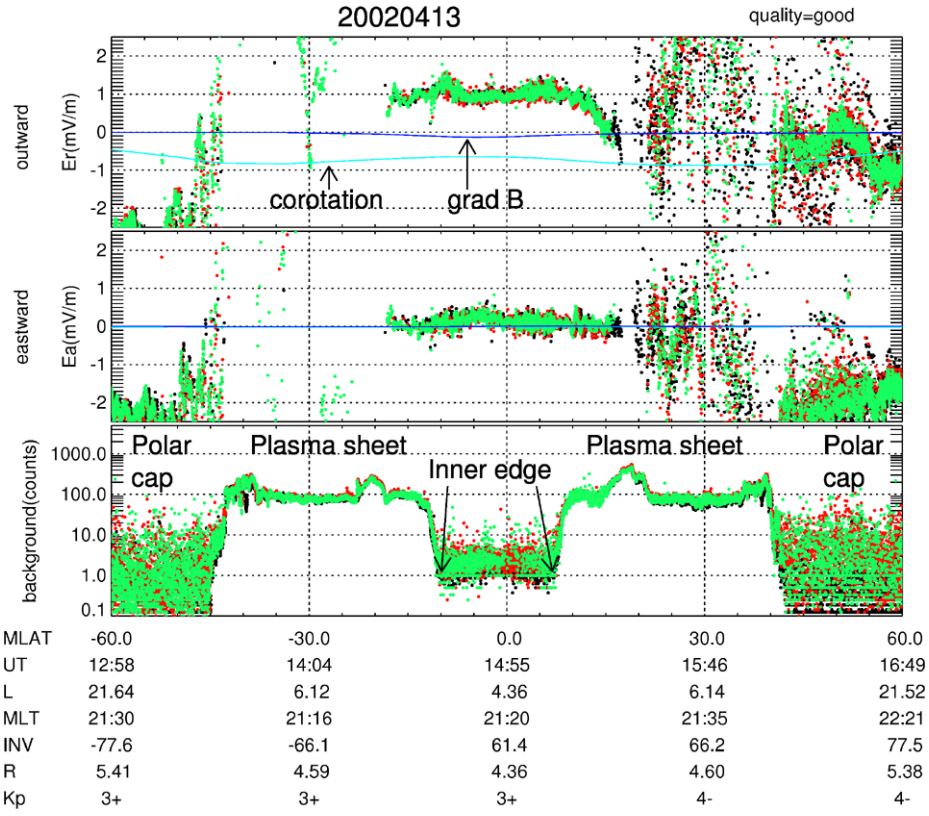

MLAT	-60.0	-30.0	0.0	30.0	60.0
UT	12:58	14:04	14:55	15:46	16:49
L	21.64	6.12	4.36	6.14	21.52
MLT	21:30	21:16	21:20	21:35	22:21
INV	-77.6	-66.1	61.4	66.2	77.5
R	5.41	4.59	4.36	4.60	5.38
Kp	3+	3+	3+	4-	4-

Fig. 4 Example of electric field measured by EDI onboard CLUSTER on 13 April 2002. Outward and eastward components of the electric field and background natural electron counts with an energy of 1 keV and a pitch angle of 90° are plotted from top to bottom. Data from C1 (*black*), C2 (*red*), and C3 (*green*) are plotted. Contributions from corotation (*light blue*), and ∇B drift (*dark blue*) are also plotted. Spacecraft plasma regimes are indicated in the *bottom panel*

and azimuthal components of the electric fields are shown in the inertial frame in the top and second panels, respectively. The electric field caused by corotating drift is shown by light blue lines so that the offset from this value shows the electric field in the corotating frame. The contribution from the ∇B drift is calculated by using the Tsyganenko-02 model (Tsyganenko 2002) and is indicated by dark blue lines: This drift is negligible with a size at most $\sim$0.1 mV m^{-1}. The bottom panel shows counts of ambient electrons with an energy of 1 keV and a pitch angle of 90°, a data product of EDI in addition to the electric field. The spacecraft are located in the polar cap, plasmasheet, and inner edge of the electron plasma sheet in this order from the high geomagnetic latitudes. The electric field is frequently measured inside the inner edge of the electron plasma sheet and in the polar cap, indicating the EDI technique is often useful. At this time, IMF B_Y and B_Z are -1.4 and -3.5 nT, respectively, in geocentric solar magnetospheric (GSM) coordinates as measured by ACE (Smith et al. 1998). The K_p index is varying from 3^+ to 4^-, indicating moderate geomagnetic activity. There is a strong outward component of electric field around perigee causing westward plasma drifts. If measured in the corotating frame, the size is as large as 1.5 mV m^{-1}. Since the location of the spacecraft is at $\sim$21:00 MLT, this electric field feature corresponds to SAPS (Foster and

Vo 2002) or SAID (Anderson et al. 2001). The detailed analysis of SAID using CLUSTER data is reviewed in Sect. 4.2. It also should be noted that the electric field includes perturbed components caused by ULF waves, for example, in the eastward component at 10–20° of MLAT. The period of these waves is ∼200 s. This case study demonstrates that common features expected in the inner magnetospheric electric field are actually measured.

2.2.2 *Statistical Studies on IMF B_Z Dependence*

It is possible to analyze the electric field statistically by using data measured by EDI onboard CLUSTER. Here, the period of data used is almost six years between February 2001 and December 2006. As CLUSTER has a polar orbit, the electric fields at spacecraft locations are mapped to the magnetic equator defined as $Z = 0$ in solar magnetospheric (SM) coordinates. The mapping is performed so that the motion of the magnetic field line at the spacecraft location is consistent with that at the magnetic equator. The parallel electric potential drop is assumed to be zero. The magnetic field model used here is the Tsyganenko-02 model (Tsyganenko 2002). Because the mapping calculation becomes increasingly computationally expensive for higher time resolution, and the present interest is on DC phenomena after eliminating contributions by ULF waves, five-minute averages are calculated before applying the mapping procedure. The mapped data are then categorized by spatial bins at $L = 4.5$–9.5 with $\Delta L = 1$ and full MLT with $\Delta MLT = 1$ hour and also polarity of IMF B_Z averaged for 40 minutes. Interplanetary data from ACE (McComas et al. 1998; Smith et al. 1998) are used with propagation delay, which is defined as X component of spacecraft position in GSE coordinates divided by solar wind speed (Matsui et al. 2004). One average value is calculated at each spatial bin for each IMF B_Z polarity. After the two-dimensional average electric field patterns are calculated, the electric potential patterns are derived using an inversion technique, as discussed fully in Matsui et al. (2004) and reviewed in Reinisch et al. (2008, this issue).

The calculated potential patterns are shown in the corotating frame in Fig. 5. Panels a and b correspond to the northward and southward IMF cases, respectively. Potential contours for southward IMF are denser than for northward IMF, indicating a strong solar wind–magnetosphere coupling effect on the inner magnetospheric electric field. This feature is consistent with the geosynchronous measurement by Baumjohann and Haerendel (1985). The electric potentials are clearly affected by M–I coupling (Vasyliunas 1970). Closure of partial ring current through the ionosphere via region 2 field aligned currents causes a skewing of equipotential contours from the Sun–Earth line (C:son Brandt et al. 2002). A uniform dawn-to-dusk convection electric field would have equipotential contours that are straight lines parallel to the Earth–Sun line. Instead, for example, the contour originating at $L = 9.5$ and 0 MLT is deflected around the Earth, as is especially noticeable for the northward IMF case. This skewing is part of the global effect of the region 2 current system that generates the shielding electric field in the ionosphere (Jaggi and Wolf 1973). There is a dawn–dusk asymmetry of the strength of the electric field, which is presumably due to the day-night asymmetry of the conductivity (Wolf 1970). Strong outward electric fields (i.e., closely-spaced equipotential contours) are observed in the evening MLT for the southward IMF case, which is consistent with SAPS or SAID structures as shown in the above case studies and by Puhl-Quinn et al. (2007). The ionospheric dynamo effect is another component seen in the pattern for the northward IMF case, at $L \sim 4$ (near perigee). This is inferred by comparing the electric field measured by CLUSTER with that obtained by ground radar at Millstone Hill (Wand and Evans 1981) and an ionospheric spacecraft DE 2 (Heelis and Coley 1992).

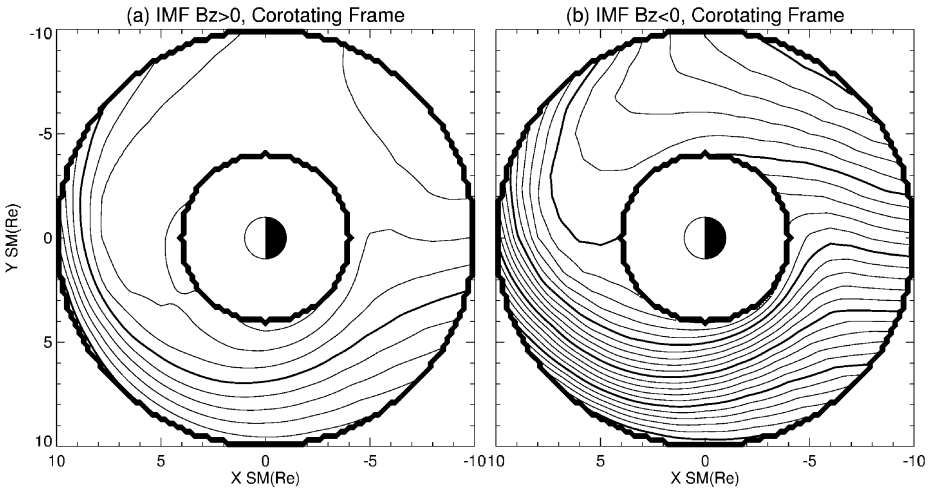

Fig. 5 Electric potential patterns derived from CLUSTER EDI data for almost 6 years. The results for (**a**) northward IMF and (**b**) southward IMF are shown in the corotating frame. Contour intervals are 1 and 5 kV for *thin and thick lines*, respectively

It should be noted that the standard deviation is often as large as the average values in the above statistics; this can be interpreted as indicating the dynamic nature of the inner magnetospheric electric fields. The motion of cold plasma is therefore expected to be complicated in the plasmasphere including at the PBL. This problem is also discussed by Pierrard et al. (2008, this issue). One factor contributing to this large standard deviation is ULF waves as shown in Fig. 4. Another factor would be the dynamic feature of substorm and/or storm activity such as undershielding and overshielding effects discussed by Huang et al. (e.g., 2006), although EDI tends to not provide data during active periods.

As mentioned above, it is confirmed that electric fields with various origins are observed: solar wind–magnetosphere interaction, M–I coupling including SAPS or SAID, ionospheric dynamo, and ULF waves. The measurement by EDI is reasonable when compared with previous studies at the ionospheric level or those based on theories. Hence, the next step is to create an inner magnetospheric electric field (UNH-IMEF) model, which is described in Matsui et al. (2008), Puhl-Quinn et al. (2008), and Reinisch et al. (2008, this issue). Electric field data measured by double probes are newly introduced to complement EDI data especially to improve data coverage during geomagnetically active periods.

In the above study, the interplanetary parameters introduced are not instantaneous ones but 40-minute averages. Here the correlation between IMF B_Z component and inner magnetospheric electric field is examined to highlight the solar-wind magnetosphere interaction. Figure 6 shows the occurrence rate of 99% correlation between the E_X and E_Y components of inner magnetospheric electric field and IMF B_Z, plotted versus the averaging interval of B_Z in the range 5 minutes to 12 hours. The correlation for E_Y is better than that for E_X because the dawn–dusk component is the primary component merged into the magnetosphere from the same component of interplanetary electric field. A peak of the correlation is obtained for a broad averaging interval of ∼20–70 minutes. The number of bins with correlations with averaging intervals >70 minutes does not decay quickly. More than half of the spatial bins (>72 bins) have significant level of correlations with averaging intervals up to 300 minutes. This would reflect the operative time

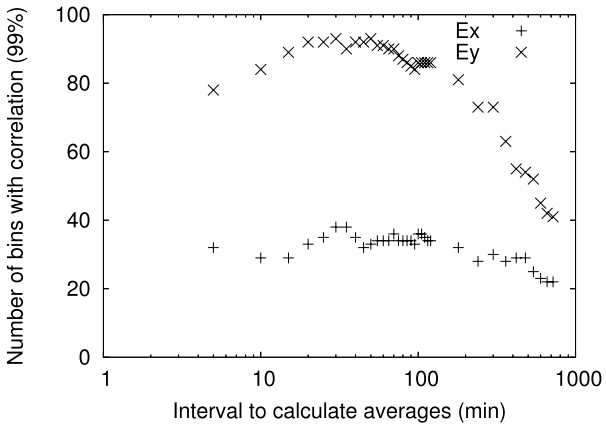

Fig. 6 Number of bins with correlation with a significant level of 99% between inner magnetospheric electric field and IMF B_Z, plotted versus the averaging interval of B_Z. E_X and E_Y components are chosen in the inner magnetosphere for 144 spatial bins (6 radial and 24 azimuthal). IMF B_Z averaging intervals between 5 minutes and 12 hours are plotted

scale of how the interplanetary medium affects the inner magnetosphere. Figure 6 demonstrates that the effect of IMF on the inner magnetospheric electric field has two relevant timescales: a prompt timescale of tens of minutes for the IMF effect to initiate an inner magnetospheric response, and a longer timescale of hours for that response to continue before decaying away. It is useful to compare CLUSTER's results from other studies investigating similar relationships. A prompt response of the plasmaspheric shape to the southward turning of IMF with a delay of a few tens of minutes was reported by Goldstein et al. (2003b). There are other reports on the prompt response ($\lesssim$10 minutes) of high latitude ionospheric electric field due to IMF B_Z changes (Ridley et al. 1998; Khan and Cowley 1999). These three studies support the response $<$1 hour. Other work by Huang et al. (2005) reported substorm recurrence periods of a few hours during continuous southward IMF, which could be related to the long term ($\sim$hours) effect of IMF. This analysis certainly suggests follow-up analysis to answer significant questions. For example, how would the IMF dependence be different for a limited area in L value and MLT? The combined effects of time delay and averaging should be investigated as well to understand the solar wind–magnetosphere interaction more clearly.

It is possible to evaluate the efficiency of the merging of the interplanetary electric field into the inner magnetosphere, which is defined by E_Y component in the inner magnetosphere divided by the same component in the interplanetary space. When the slope of the relation between the IMF B_Z component and E_Y component in the inner magnetosphere is calculated, the average and standard deviation are -0.05 ± 0.03 (mV m^{-1}) nT^{-1}. If a typical solar wind speed of 450 km s^{-1} is introduced, the efficiency is 0.11 ± 0.07. This value is comparable to that estimated by Goldstein et al. (2003b) as 0.12 from an IMAGE EUV observation.

2.2.3 Statistical Studies on IMF B_Y Dependence

In addition to the IMF B_Z component, the electric field in the polar cap region is known to be affected by IMF B_Y (e.g., Cowley 1981; Heppner and Maynard 1987) and season (e.g., de la Beaujardiere et al. 1991; Crooker and Rich 1993). Both IMF B_Y and seasonal effects are expected to appear oppositely in the northern and southern hemispheres. For example, the potential pattern with positive IMF B_Y (in June) in the northern hemisphere is the same as that with negative IMF B_Y (in December) in the southern hemisphere. Whether this seasonal asymmetry effect is preserved or canceled near the magnetic equator in the

inner magnetosphere was examined at geosynchronous orbit by Baumjohann et al. (1986). Extending this work, Matsui et al. (2005) compared the electric fields between northern and southern hemispheres and found some north-south disparity, especially on the dawn side, a result consistent with the expectation in the polar region by the Weimer model (Weimer 2001). Thus, the electric field in the region of the inner magnetosphere covered by CLUSTER's orbits is subject to a IMF B_Y dependence that is similar to that found in the polar region. From this result may be inferred a seasonal variation of M–I coupling, a reasonable inference because of the seasonal variation of ionospheric conductivity.

2.3 Summary

Measurement of the inner magnetospheric electric field by EDI onboard CLUSTER has been reviewed in this section, based on studies by Matsui et al. (2003, 2004, 2005). The electric fields show various features such as solar wind–magnetosphere interaction, M–I coupling including SAPS or SAID, ionospheric dynamo, and ULF waves. Analyses of the solar wind–magnetosphere interaction have also been reviewed: IMF B_Z dependence of the potential patterns sorted by its polarity, correlation time scale by averaging IMF B_Z, and efficiency of merging. Observation by CLUSTER of IMF B_Y and seasonal dependence in the inner magnetosphere reflects that the condition of both solar wind and ionosphere can have an effect. Given recent progress in observational characterization of the electric field, the next step should be to develop a convection electric field model. Such a model would be useful for studies of both plasmasphere and ring current dynamics (Reinisch et al. 2008, this issue).

3 Inner Magnetospheric Electric Fields From Plasmasphere Images

3.1 Technique for Deducing Electric Fields From IMAGE

Inspired by earlier work that inferred cross-L drifts by tracking the motion of whistler ducts (Carpenter and Seely 1976), the motion of the plasmapause boundary in IMAGE EUV plasmasphere images has been used to deduce the electric field along the plasmapause (Goldstein et al. 2004b). This technique relies on the assumption that the boundary motion results from the $\boldsymbol{E} \times \boldsymbol{B}$ drift of cold plasmaspheric plasma at (or just inside) the plasmapause. For a relatively smooth, featureless plasmapause it is only possible to infer the tangential electric field component. However, convection often produces indentations and bulges whose motion along the boundary can be tracked, allowing a limited capability to obtain two vector electric field components (Goldstein et al. 2004a, 2005b). More recently, some effort has gone into more sophisticated analysis of an entire EUV image, in an attempt to track plasma motion inside the entire plasmasphere (not just at the plasmapause) and obtain a full two-dimensional vector flow (i.e., electric) field (Gallagher and Adrian 2007; De Keyser et al. 2008, this issue).

3.2 Phenomenology of the Erosion Process

Though the electric fields deduced from analysis of EUV images are somewhat crude (both in spatial and temporal resolution) relative to that provided by in situ measurements, global snapshots of the inner magnetospheric electric field have yielded some important observations about the erosion process. Several studies have shown a strong correlation between erosion and southward IMF in the solar wind, but there is a 20–30 minute time delay between the arrival of southward IMF at the dayside magnetopause

and the subsequent onset of erosion (Goldstein et al. 2003a; Spasojević et al. 2003; Goldstein 2006). Different MLT sectors of the plasmapause respond at different times, possibly owing to the finite $\boldsymbol{E} \times \boldsymbol{B}$ drift speed of eroding plasma (Larsen et al. 2007). Nightside erosion begins as an initial indentation a few MLT hours wide, centered at or east of midnight; this indentation expands both eastward and westward, widening to eventually encompass the entire nightside (Goldstein et al. 2004b; Goldstein and Sandel 2005; Gallagher and Adrian 2007). The substorm response is similar to that of erosion, but more transient; ripples propagate both eastward and westward from a common initial indentation, but after the passage of a ripple past a given MLT the plasmapause can recover its initial location (Goldstein et al. 2005b). The erosion process is described in more detail elsewhere in this issue (Darrouzet et al. 2008).

3.3 Internal Magnetospheric Electric Fields

The availability of plasmasphere images has facilitated significant progress in understanding electric fields that originate internally in the magnetosphere (as opposed to being directly driven by the solar wind–magnetosphere interaction). These internal electric fields are generated when the stormtime partial ring current is closed through the ionosphere via region 2 field-aligned currents (FAC). Two main types of internal electric fields have been investigated using IMAGE EUV: shielding and SAPS.

In shielding, ionospheric current closure produces an eastward electric field that counters the global dawn-to-dusk solar-wind-driven convection field (Jaggi and Wolf 1973). Images of the plasmasphere during times of changing convection strength indicate that there is generally a dynamic imbalance between convection and shielding (Goldstein et al. 2002, 2003c; Wolf et al. 2005; Sazykin et al. 2005). These images provide a convincing global contextual picture for observations from the inner magnetosphere (earthward of the stormtime ring current) and low-latitude ionosphere (equatorward of the region 2 currents) (Fejer et al. 1990; Fejer and Scherliess 1995; Scherliess and Fejer 1997; Rowland and Wygant 1998; Wygant et al. 1998) that had seemed to refute the idea of a perfectly shielded, quiescent inner magnetosphere.

SAPS is a broad region of westward flow enhancement generated by a poleward Pederson current in the low-conductivity region equatorward of the electron aurora (Anderson et al. 2001; Foster and Burke 2002). The broad SAPS region often contains a sharp intensification of westward flow that is called SAID or polarization jet (PJ); SAID/PJ may be considered a special limiting case of SAPS, although at times (in the literature) SAPS and SAID have been used interchangeably. Stormtime plasmasphere images have provided a means of studying the effects of SAPS on cold plasma. IMAGE observations showed the degree to which SAPS can intensify erosion at the duskside edge of plumes and move the plume location earthward (Goldstein et al. 2003b, 2005c), and enabled the creation of magnetospheric models of the SAPS electric field (Goldstein et al. 2005a, 2005c). During substorms, rapid growth of SAPS electric fields can produce undulatory motion of the plasmapause (Goldstein et al. 2004a, 2007). Extraction of electric fields from plasmapause undulations have provided quantitative global measurements of SAPS in the inner magnetosphere that complement low-altitude measurements by satellites such as DMSP (Goldstein et al. 2004a, 2005b). More about SAPS fields is found in the next section.

4 SAPS Electric Fields

4.1 DMSP and IMAGE Observation

During storms, the effects of magnetospheric electric fields and $\boldsymbol{E} \times \boldsymbol{B}$ plasma convection extend deep into the mid-latitude ionosphere producing dramatic effects. At the PBL, strong electric fields associated with storm-time ring current enhancement contribute to the formation of the deep mid-latitude ionospheric density trough and the erosion of the overlying plasmasphere. This process is associated with M–I coupling and ionospheric feedback in the region where magnetospheric FACs attempt to close across the low-conductance subauroral ionosphere. The potential distribution required to satisfy current continuity across this region is adjusted to reflect ionospheric conditions, and maps back into the magnetosphere along magnetic field lines (Nopper and Carovillano 1978).

Foster and Burke (2002) and Foster and Vo (2002) provide a brief description of this process, which is consistent with the model for SAID discussed by Anderson et al. (1993) and others. As disturbance electric fields energize ring-current particles and transport them into the inner magnetosphere, large pressure maxima develop in the nightside magnetosphere. Finite gyroradius effects, intensified by shear flows, may create intense localized transverse electric fields (De Keyser et al. 1998; De Keyser 1999). Misalignments between gradients in plasma pressure and magnetic flux tube volume cause region 2 FACs to flow into/out of the ionosphere evening/morning sector. A fraction of region 2 FACs flow into regions of low ionospheric conductivity at sub-auroral latitudes where large polarization electric fields, needed to maintain current continuity, drive the rapidly drifting streams of storm enhanced density (SED) (Foster 1993) which are the ionospheric signature of the plasmasphere erosion plumes imaged by IMAGE EUV (e.g., Sandel et al. 2001). Within the region of strong plasma drifts frictional heating enhances ionospheric recombination rates (Schunk et al. 1976), accelerating the reduction of ionospheric conductivity in the channel. This, in turn, increases the intensity of the polarization electric fields, leading to still deeper ionospheric troughs and more rapid plasma flow in both the ionosphere and magnetosphere.

Large potential drops imposed on the magnetosphere and polar ionospheres by the solar wind-driven convection electric fields are the ultimate drivers of the SAPS. Region 1 FACs drawn from the interplanetary generator flow near the poleward boundary of the auroral oval; into the ionosphere on the dawn side and out of the ionosphere on the dusk side. The potential distribution required to satisfy Ohm's Law spans the global ionosphere, is adjusted to reflect ionospheric conditions, and maps back into the magnetosphere along magnetic field lines (Nopper and Carovillano 1978).

The SAPS has considerable consequences on the dynamics and redistribution of thermal plasma within the coupled inner magnetosphere/ionosphere system. Anderson et al. (2001) have demonstrated that the SAID electric fields are magnetically conjugate and extend along magnetic field lines into the magnetosphere. The overlap of SAPS with the plasmasphere (see Fig. 7) erodes its outer layers to form the steep disturbed-time plasmapause and spectacular plasmaspheric tails which have been imaged with the EUV detector on the IMAGE satellite (Foster et al. 2002, 2007). Figure 7 and the study of Foster et al. (2007) demonstrate that the SAPS channel, measured at lower altitude by the DMSP satellites in the topside ionosphere, maps upward to the apex of the magnetic field where it accounts for the strong sunward flow which erodes the outer plasmasphere, drawing out the plasmaspheric plumes seen by IMAGE and CLUSTER (Darrouzet et al. 2008, this issue).

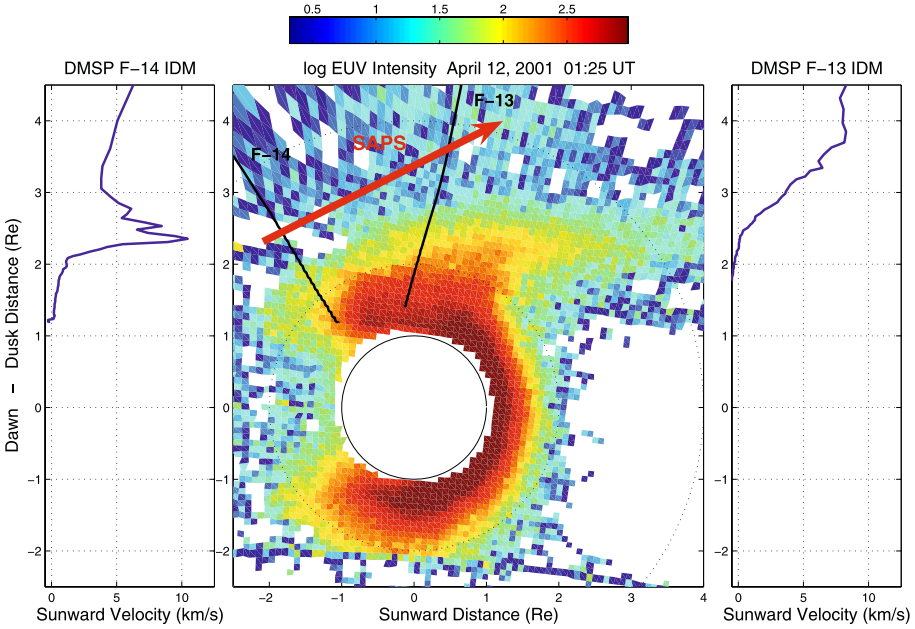

Fig. 7 The IMAGE EUV "snapshot" of the plasmasphere and drainage plume has been mapped to the GSM equatorial plane (Tsyganenko 2002, magnetic field mapping). DMSP passes locate the SAPS channel immediately outside and adjacent to the plasmasphere drainage plume. At dusk, the inward extent of the SAPS sunward convection velocity observed by DMSP F-13 overlaps the outer portion of the IMAGE EUV erosion plume. (Adapted from Foster et al. 2007)

4.2 Multi-Spacecraft Observations of SAID: A CLUSTER Perspective

Conjugate, multi-spacecraft observations of the inner M–I coupling phenomena known as SAID present the opportunity to study how the coupling is created and maintained along entire magnetic flux tubes connecting the southern to the northern ionosphere. Ionospheric observations of SAID are quite extensive, and date back to the mid-1970s (e.g., Galperin et al. 1974; Smiddy et al. 1977; Spiro et al. 1979; Karlsson et al. 1998; Foster and Vo 2002; Figueiredo et al. 2004). Conjugate ionosphere-magnetosphere observations of SAID, however, are relatively rare due to the typical long-period orbit of magnetospheric satellites, which produces a relatively low probability for both the ionospheric and magnetospheric satellites to be in the "right place at the right time".

4.2.1 SAID Electric Field

Figure 8 summarizes the three known conjugate ionospheric–magnetospheric, multi-spacecraft studies of SAID to date. In the pioneering work of Anderson et al. (2001), conjugate, in situ, magnetospheric and ionospheric observations of SAID were presented for the first time (Fig. 8a). Depicted in this figure is a summary of information extracted from their Fig. 1a. Plotted are peak electric field vectors (arrows) occurring within the SAID channel on 7 February 1990. These electric field vectors are meridional (causing westward drift), and lie within the meridional plane intersecting 21:43 MLT (i.e., the plane of the plot, the X–Z DMS or dipole meridian system plane, is the meridional plane intersecting

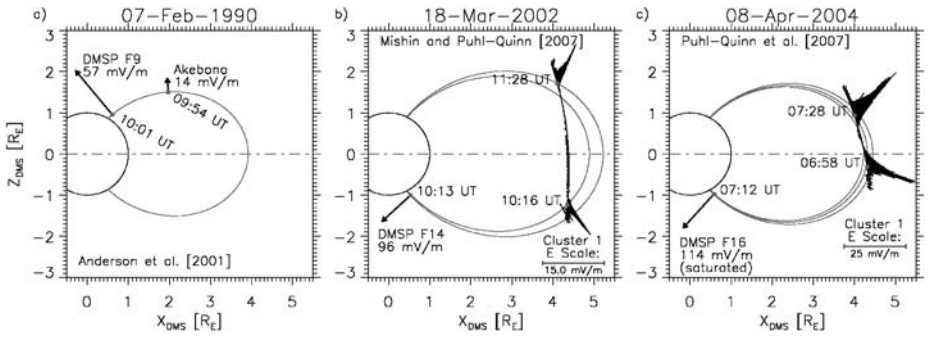

Fig. 8 Multi-spacecraft observations of SAID meridional electric field vectors measured by DMSP, AKEBONO, and CLUSTER. Panels **a**–**c** show meridional electric field vectors measured by various spacecraft for three events: (**a**) 7 February 1990, (**b**) 18 March 2002 and (**c**) 8 April 2004. From left to right, the X_{DMS}–Z_{DMS} plane is the meridional plane intersecting 21:43, 23:00, and 21:45 MLT, respectively. Dipolar magnetic field lines are drawn for reference. Electric field vectors are drawn either at specific times (for DMSP and AKEBONO) or at several times along the spacecraft orbit (for CLUSTER). Panel **a** shows a summary of information extracted from Fig. 1a of Anderson et al. (2001), where DMSP F9 and AKEBONO were magnetically conjugate at ∼10:00 UT and measured SAID electric fields. Panel **b** summarizes the case study presented by Mishin and Puhl-Quinn (2007), where DMSP F14 and CLUSTER were magnetically conjugate in the southern hemisphere at ∼10:15 UT. Panel **c** summarizes the case study presented by Puhl-Quinn et al. (2007) where DMSP F16 and CLUSTER made conjugate SAID measurements

21:43 MLT). The SAID channel is observed at both DMSP F9 (∼835 km altitude) and AKEBONO (∼9400 km altitude). The field-aligned separation of these conjugate observations is ∼9700 km. A dipolar field line for $L = 3.9$ (invariant latitude, ILAT = 59.7°) is drawn to illustrate the magnetic conjugacy of the two spacecraft. The in situ electric field peak at DMSP F9 (AKEBONO) is 57 (14) mV m^{-1}. These values are consistent with the absence of any appreciable field-aligned potential difference between the two spacecraft.

With CLUSTER, we have the opportunity to observe SAID closer to the magnetic equatorial plane. It is fortuitous that typical SAID electric fields at ionospheric heights map to easily measurable electric field magnitudes in the magnetosphere. For example, at $L = 4$ (ILAT = 60°), westward ionospheric drifts of 1.0, 2.0 and 3.0 km s^{-1}, corresponding to poleward-directed electric fields of 38, 77 and 115 mV m^{-1}, respectively, electrostatically map to the magnetic equator as radially outward electric fields of 2.7, 5.3 and 8.0 mV m^{-1}, respectively.

Figures 8b and c show multi-spacecraft observations of SAID during the CLUSTER era. The format is the same as that of Fig. 8a, except that the meridional planes depicted in b and c are those intersecting 23:00 and 21:45 MLT, respectively. In both cases, CLUSTER observes the SAID channel in both hemispheres, and DMSP observations are in the southern hemisphere. The field-aligned separation in Fig. 8b between C1 at 10:16 UT and DMSP F14 at 10:13 UT is ∼25711 km, more than a factor of two larger than that in Fig. 8a between DMSP F9 and AKEBONO. At this time (10:16 UT), C1 is located 15° below the magnetic equator. It was shown in Mishin and Puhl-Quinn (2007) that the electrostatically mapped CLUSTER value of ∼10 mV m^{-1} agrees to within 10% of the DMSP value of ∼100 mV m^{-1}, again indicated no appreciable field-aligned potential difference between the magnetospheric and ionospheric locations. The field-aligned separation is extended even further in Fig. 8c, with 27561 km between C1 at 06:58 UT, and DMSP F16 at 07:12 UT. C1 is a mere 4° below the magnetic equator in this case. Nonetheless, a strong SAID signature is observed, indicating the existence of the SAID channel along the entire fieldline. As described in Puhl-Quinn

et al. (2007), a magnitude comparison was not possible, because the DMSP F16 drift meter became saturated within the channel. The strong ~25 mV m^{-1} fields measured at CLUSTER would electrostatically map to over 300 mV m^{-1} at DMSP altitude, whereas the DMSP drift meter saturated at 114 mV m^{-1}.

4.2.2 SAID Field-Aligned Current

In addition to the coherent SAID electric field channel illustrated in Fig. 8, another large-scale feature of this M–I coupled system is FAC. It has been routinely shown that FAC flows both into and out of the topside ionosphere in the vicinity of SAID (e.g., Rich et al. 1980; Anderson et al. 2001). The ionospheric SAID FAC morphology and strength are quite variable, which is attributed to the dynamic response of the ionospheric conductivity during the initial development and subsequent evolution of the SAID channel. Application of electrical current continuity to the topside ionosphere, under simplifying assumptions, and in the assumed absence of large horizontal conductivity gradients, reveals a possible initial configuration of two, oppositely directed FAC sheets supporting the electric field gradients at the edges of the SAID channel (e.g., Puhl-Quinn et al. 2007). However, this is rarely observed due to the fact that conductivity gradients are relatively quickly formed and serve to support the electric field gradients rather than FAC. The time history of ionospheric SAID FAC morphology relative to the SAID electric field morphology is, in fact, used to formulate hypotheses regarding the magnetosphere's role as a current and/or voltage generator (e.g., Anderson et al. 1993, 2001). More recently, Figueiredo et al. (2004) found that there is evidence to support both types of generator. And Mishin and Puhl-Quinn (2007) used CLUSTER and DMSP data to show that the overall SAID features are consistent with a short circuiting of the substorm injection front over the plasmasphere and subsequent formation of a turbulent overlap region.

Diagnosing the SAID FAC signature at magnetospheric heights was attempted for the first time using CLUSTER data (Mishin and Puhl-Quinn 2007; Puhl-Quinn et al. 2007). The main challenge in the magnetosphere is to successfully isolate the SAID-related current structure, which is embedded in a complex superposition of magnetic perturbations. Using a standard spline/pchip procedure, Mishin and Puhl-Quinn (2007) were able to fit large-scale magnetic components around the channel, and subtract them from the total field in order to isolate the SAID-related FAC structure. Values for in situ SAID FAC within the channel exceed 10 nA m^{-2} for both the 18 March 2002 and 08 April 2004 events. Magnetic lensing of the FAC (assuming $\nabla_\perp \boldsymbol{j}_\perp = 0$ along the flux tube) yields values on the order of 1.3 and 0.57 μA m^{-2} for the 2002 and 2004 events, respectively. The ionospheric in situ values are 0.5 and 0.3 μA m^{-2}, respectively. This trend for the lensed magnetospheric FAC values to be larger than their in situ ionospheric counterparts indicates that partial closure of the FAC occurs between DMSP and CLUSTER altitudes. A more comprehensive and rigorous analysis of several DMSP/CLUSTER conjugations is underway in order to confirm this hypothesis.

5 Spatial Gradients of the Magnetic Field in the Plasmasphere from CLUSTER

The CLUSTER mission allows study of the global orientation of plasmaspheric fields with four-point measurements. Darrouzet et al. (2006) and De Keyser et al. (2007) have analyzed a typical plasmasphere crossing by CLUSTER for this purpose; this work has been limited to computing derivatives of the magnetic field. This also allows the evaluation of $\nabla \times \boldsymbol{B}$, which is proportional to the electric current density (Vallat et al. 2005; Dunlop et al. 2006), at least if there are no rapid time variations, and to check $\nabla \cdot \boldsymbol{B}$, which should be zero.

5.1 Datasets and Analysis Technique

The physical quantity used in this study is the spin average DC magnetic field components measured by FGM (Balogh et al. 2001). The uncertainty on those data is less than 0.1 nT. To verify and interpret the results, Darrouzet et al. (2006) have also used a model magnetic field that combines the internal magnetic field model IGRF2000 and the external Tsyganenko-96 magnetic field model (Tsyganenko and Stern 1996).

Techniques to compute the gradients of scalar and vector quantities along the trajectory of the center of the CLUSTER tetrahedron have been introduced by Harvey (1998) (instantaneous spatial gradient computation) and by De Keyser et al. (2007) (least-squares gradient computation), and are described elsewhere in this issue (De Keyser et al. 2008). A prime condition for these methods to work properly is the hypothesis that the satellites are close enough to each other, so that all spacecraft are embedded in the same structure at the same time (homogeneity condition), although this condition can be relaxed somewhat for the least-squares gradient technique. The least-squares gradient technique requires exactly four non-coplanar points to compute the gradient of a scalar quantity or individual vector components. For the magnetic field, the gradients of the field components can be computed, and from them the divergence and the curl, leading to the so-called curlometer method for computing the current density. The least-squares technique imposes strict constraints, such as the divergence-free condition for the magnetic field, thereby leading to an improved curlometer. The technique provides total error estimates on the gradient (and the divergence and the curl).

5.2 A Typical Plasmasphere Crossing

Consider the plasmasphere crossing on 7 August 2003, between 07:00 and 09:00 UT, at 14:00 LT and between -30 and $+30^\circ$ of MLAT during a geomagnetically moderately active regime, which has been analyzed by Darrouzet et al. (2006). At that time, the spacecraft separation was small and the tetrahedron geometric factors are satisfactory. From the measurement errors, and by estimating the approximation error on the gradient (related to the homogeneity condition), the total error on the field magnitude gradient is judged to be about 5%. For the same event, De Keyser et al. (2007) have computed both the gradient ∇B and the gradients of the individual components of $\boldsymbol{B}$ using the least-squares technique.

In order to study the orientation of the gradient, it is useful to compare its direction to that of the local magnetic field. The angle between the gradient ∇B with respect to the local magnetic field $\boldsymbol{B}$ (at the center of the tetrahedron) is called $\alpha_{\boldsymbol{B},\nabla B}$. This angle is always in the range between 0 and 90°, because one is only interested in the orientation of the gradients, and not in their sense, and is known up to a precision of about 3°. The global orientation of the magnetic field strength gradient is also described by its latitude $\theta_{\nabla B}$ and its azimuth relative to the spacecraft azimuth angle $\phi_{\nabla B} - \phi_{\rm sc}$. The precision is 3° on $\theta_{\nabla B}$ and $\phi_{\nabla B} - \phi_{\rm sc}$. In a completely analogous way, angle $\alpha_{\boldsymbol{B},j}$ can be defined to study the orientation of the current density vector $\boldsymbol{j}$, which is proportional to $\nabla \times \boldsymbol{B}$, with respect to the magnetic field. Figure 9a displays the electron density determined by the WHISPER (Waves of HIgh frequency and Sounder for Probing Electron density by Relaxation) instrument (Décréau et al. 2001) onboard the four CLUSTER spacecraft as a function of time. Figure 9b gives the angle $\alpha_{\boldsymbol{B},\nabla B}$. The latitude angle $\theta_{\nabla B}$ and azimuth angle $\phi_{\nabla B} - \phi_{\rm sc}$ of the gradient of the observed FGM magnetic field strength (solid curves) and of the IGRF-Tsyganenko model field strength (dashed curves) are given in Fig. 9c–d.

The magnetic equator is defined as the surface of minimum field strength locations along field lines. It is crossed where $\boldsymbol{B}$ and ∇B are perpendicular, i.e., when $\alpha_{\boldsymbol{B},\nabla B} = 90^\circ$. This

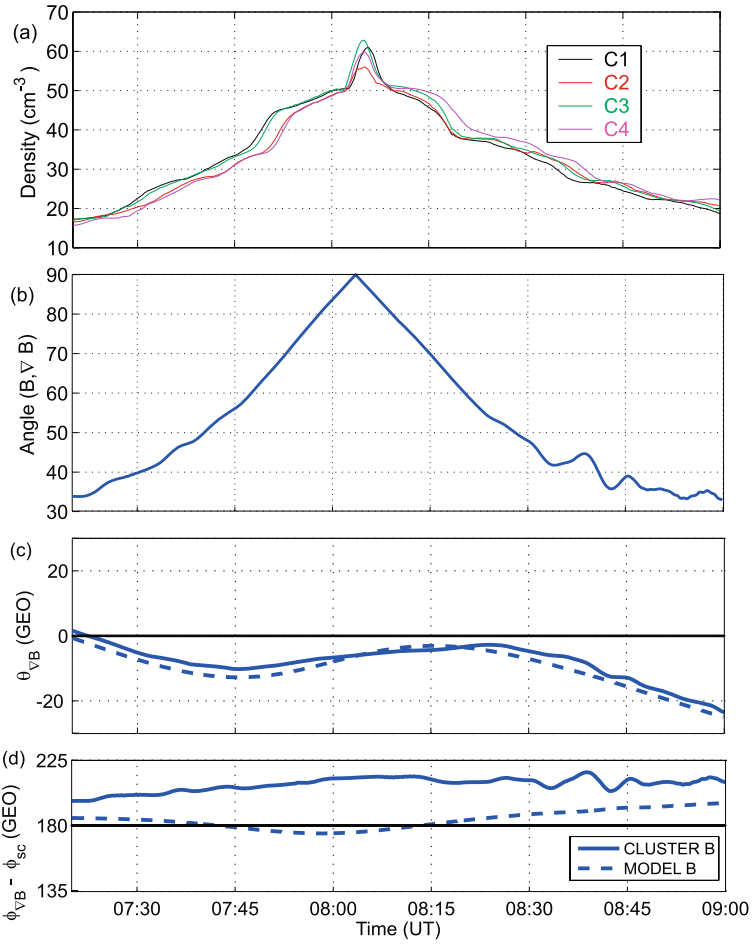

Fig. 9 (**a**) Electron density from WHISPER onboard the four CLUSTER spacecraft, (**b**) angle $\alpha_{\boldsymbol{B},\nabla B}$ between the magnetic field strength gradient ∇B and the local field $\boldsymbol{B}$, and (**c**) latitude angle $\theta_{\nabla B}$ and (**d**) azimuth angle $\phi_{\nabla B} - \phi_{\rm sc}$ of ∇B, as a function of time during the plasmasphere crossing on 7 August 2003. The angles are known up to about 3°. The gradients based on CLUSTER data are represented by the *solid lines*, while gradients computed from the IGRF-Tsyganenko model are drawn with *dashed lines*. (Adapted from Darrouzet et al. 2006)

allows an unambiguous identification of the time of crossing of the magnetic equator in Fig. 9b at 08:03 UT. Note that this in general does not coincide with the time of perigee (08:20 UT) or with the time of maximum density (08:05 UT), but there is not much difference in the present case. Before and after crossing the magnetic equator, the spacecraft sample field lines farther away from the equator and $\alpha_{\boldsymbol{B},\nabla B}$ decreases as B increases along a field line in the poleward direction in a progressively steeper fashion. Far from the magnetic equator, $\alpha_{\boldsymbol{B},\nabla B}$ becomes more variable: In the outer fringes of the plasmasphere, the magnetic field strength is smaller and plasma β is higher, which could enhance diamagnetic effects.

For both the observed magnetic field (FGM data) and the model field (IGRF-Tsyganenko), the values of $\theta_{\nabla B}$ are comparable: They vary between 0 and $-20°$. For a tilted dipole (tilt of 10.3° at 71.7°W longitude in 2003), at 08:03 UT and 14:00 LT, the magnetic equator should be at a latitude of 10°; the spacecraft encounter the magnetic equator at $\theta_{sc} = 8.5°$. At the magnetic equator of an exact dipole, ∇B would point earthward, so that $\theta^{eq}_{\nabla B} = -\theta_{sc}$; at the actual magnetic equator, the observed value is $\theta^{eq}_{\nabla B} = -6°$.

When the CLUSTER spacecraft cross field lines at higher latitude, the variation of $\theta_{\nabla B}$ depends on how fast B increases away from the magnetic equator. Figure 9b indicates that $\alpha_{\boldsymbol{B},\nabla B}$ decreases rapidly, so that $\theta_{\nabla B} > \theta^{eq}_{\nabla B}$ just above the magnetic equator and $\theta_{\nabla B} < \theta^{eq}_{\nabla B}$ just below it. But since the field lines are curved towards the Earth farther away from the equator, ultimately $\theta_{\nabla B} \ll \theta^{eq}_{\nabla B}$ at higher latitudes above the magnetic equator and $\theta_{\nabla B} \gg \theta^{eq}_{\nabla B}$ below it. The actual behavior of $\theta_{\nabla B}$ is determined by the geometry of the field lines and by the interplay between the variation of B along field lines ($\nabla_{\parallel} B$) and its variation across field lines ($\nabla_{\perp} B$), offset by the overall dipole tilt.

The azimuth of the observed field strength (FGM data) is $\phi_{\nabla B} - \phi_{sc} \approx 200°$, while it is around 180° for the model field (IGRF-Tsyganenko). If the magnetic field would be a tilted dipole, one would expect $\phi_{\nabla B} - \phi_{sc} = 180°$ at the magnetic equator. The IGRF-Tsyganenko model represents a modified tilted dipole, and indeed has $\phi_{\nabla B} - \phi_{sc}$ close to 180°, i.e., exactly pointing towards Earth. The observed azimuth angle of 200° can only be explained by a deviation from cylinder symmetry around the dipole axis.

These results are confirmed by an analysis with the least-squares gradient computation technique (De Keyser et al. 2007), as summarized in Fig. 10 for a somewhat longer time interval. The magnetic field strength profiles are shown to go through a local minimum near perigee (Fig. 10a). A computation of the angle between $\boldsymbol{B}$ and ∇B (see Fig. 10b), using realistic input for the error estimates, produces a curve that is very similar to the one of Fig. 9b. The error bars are quite small close to the magnetic equator but they increase significantly away from the equator. There are several reasons: The relative precision of the data is lower there since B is smaller, and the differences between the values measured by the spacecraft are smaller (the gradient itself is smaller). The absence of gradient values in the interval 09:30–09:45 and the very large error bars nearby are due to the bad configuration of the spacecraft: They are nearly coplanar, with the plane containing the spacecraft velocity vector, which is responsible for a bad conditioning of the problem, so that no useful results can be obtained there. For details of the computation, the reader is referred to De Keyser et al. (2007).

Figures 10c and d show the results of a least-squares computation of the gradients of the magnetic field vector components, coupling the three field components through the zero-divergence constraint. The angle $\alpha_{\boldsymbol{B},\boldsymbol{j}}$ between $\boldsymbol{B}$ and current density $\boldsymbol{j}$ (where $\boldsymbol{j} = \nabla \times \boldsymbol{B}/\mu_0$ in a steady situation) can vary in principle between 0° and 180°. It is around 90° near the equator, as expected for a roughly symmetric situation. The current density $\boldsymbol{j}$ appears to be different from zero in the plasmasphere, indicating deviation from a dipolar field, with a field-aligned component inside the plasmasphere (around perigee) and also on auroral field lines (just after 06:00 UT). The relative error is on the order of 5–10% on j near perigee, and 5–10° on $\alpha_{\boldsymbol{B},\boldsymbol{j}}$, and grows away from the equator for the reasons discussed before. It should be noted, however, that the error bars are drawn at 1 standard deviation and are determined using a rough a priori estimate of the homogeneity properties. A further assessment of the statistical significance of these results is therefore needed. The seemingly erratic values close to the coplanarity interval carry very large error bars and must be ignored. De Keyser et al. (2007) have performed this computation both with and without imposing the condition $\nabla \cdot B = 0$; they find that this does not affect $\boldsymbol{j}$ very much, since divergence and curl both involve different derivatives. This conclusion probably depends on

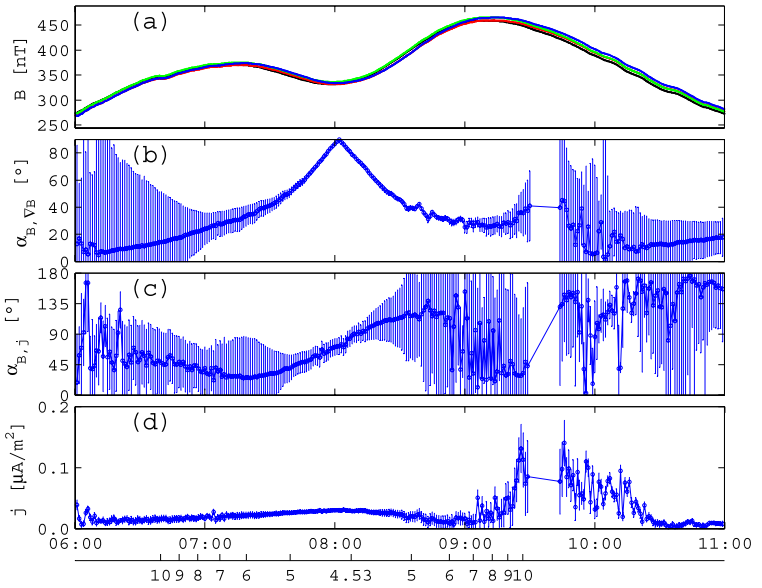

Fig. 10 CLUSTER observations during the inner magnetosphere pass on 7 August 2003, from 06:00 to 11:00 UT, with perigee around 08:03 UT; the bottom scale gives the L-shell position of the center of the CLUSTER tetrahedron (for $L < 10$, elsewhere L cannot be determined accurately). (**a**) Magnetic field strength B obtained from FGM, reaching a local minimum near perigee, C1—*black*, C2—*red*, C3—*green*, C4—*blue*. (**b**) Angle $\alpha_{\boldsymbol{B},\nabla B}$ between $\boldsymbol{B}$ and ∇B (computed with anisotropic homogeneity domain, assuming small-scale fluctuations are present), reduced to $[0°, 90°]$. (**c**) Angle $\alpha_{\boldsymbol{B},\boldsymbol{j}}$ between $\boldsymbol{B}$ and current density $\boldsymbol{j}$ (where $\boldsymbol{j} = \nabla \times \boldsymbol{B}/\mu_0$ in a steady situation). (**d**) Current density magnitude j. The *error bars* are determined using an estimate of the homogeneity properties, so they are only approximate. (Adapted from De Keyser et al. 2007)

the actual spacecraft separation distance involved, but reflects the typical CLUSTER situation in the plasmasphere.

5.3 Summary and Conclusions

CLUSTER has provided the first systematic spatial gradient results in the plasmasphere, using well-calibrated, unbiased measurements. This produces an overall view of the geometry of the magnetic field in the (outer) plasmasphere. It allows the evaluation of the relative importance between the two effects influencing the spatial gradient of the magnetic field strength inside the plasmasphere: the increase of the magnetic field strength along the field lines away from the equator, and the decrease of this quantity away from Earth.

The variations of the magnetic field strength along the field lines are rather fast, with $|\nabla_{\parallel} B| > |\nabla_{\perp} B|$ (except very close to the magnetic equator). The latitudinal magnetic field structure is found to be roughly compatible with a tilted dipole, but there appear to be significant deviations from cylindrical symmetry. The analysis of electric current density points also toward such a symmetric structure, but the finding of a small, marginally significant nonzero current density indicates again a deviation from the simple tilted dipole model.

It should also be noted that CLUSTER sometimes does observe diamagnetic effects due to the presence of the plasmaspheric plasma, in the form of minor magnetic field strength depressions corresponding to density structure in the outer regions of the plasmasphere, but

it is hard to establish a precise relationship due to the unmeasured contribution of the ring current and radiation belt plasma pressures.

6 Summary and Outlook

Various aspects of plasmaspheric electric fields and magnetic fields have been reviewed in this paper. Ground-based measurements of lightning-generated whistlers and signals from transmitters made it possible to derive electric fields inside the plasmasphere by probing the movement of density ducts. Since the 1960s these whistler studies have provided a context and motivation for later work. Modern observation (e.g., by CLUSTER/IMAGE) of quiet-time, substorm, and SAPS-generated electric fields are entirely consistent with the earlier whistler observations. The CLUSTER and IMAGE missions (launched in 2000) have both improved substantially our capabilities in measuring electromagnetic fields in the plasmasphere. In particular, multiple spacecraft analysis, improved electric field measurements, and tracking the motion of global boundaries were not possible with data from previous missions. The following four points are major achievements from these new satellite measurements.

1. EDI onboard CLUSTER measures electric fields successfully in the inner magnetosphere. Electric fields with various origins are analyzed. In particular, the electric field is examined in terms of the solar wind–magnetosphere interaction.
2. By adapting whistler-based techniques for inferring cross-L drifts, IMAGE EUV plasmasphere images can be analyzed to yield 1- or 2-component electric field information near the plasmapause (and possibly within the plasmasphere). These IMAGE-derived electric fields have helped quantify the temporal (and likely causal) correlation between southward IMF and plasmasphere erosion. Images show that the erosion process is initiated at different times depending on the MLT. Erosion begins as an indentation a few MLT hours wide that widens to encompass the entire plasmapause at all MLTs. During substorms, the starting indentation propagates to other MLTs, but the plasmapause can recover its initial location once the transient disturbance has passed. IMAGE data have also improved our quantitative understanding and models for shielding and SAPS.
3. SAPS or SAID features are observed simultaneously by IMAGE, CLUSTER, and DMSP. This gives a detailed picture of their influence on the PBL. IMAGE/DMSP and ground-based observations have shown that the SAPS convection overlaps the PBL and draws out the erosion plume which forms the outer boundary of the eroding plasmasphere in the dusk sector. Conjugate, in situ CLUSTER/DMSP observations have confirmed that the scale of the electric field and FAC structure within the SAID channel extends from one ionosphere to the other, that there are no appreciable potential drops over this extent, and that partial current closure is expected to exist between DMSP and CLUSTER altitudes.
4. The gradient of the magnetic field is calculated using data from multiple CLUSTER satellites. This will be useful for future field-aligned current and ring current studies.

CLUSTER and IMAGE revealed many dynamic characteristics of the plasmasphere as noted above. It is possible to discuss these results in the context of the whistler measurements introduced in Sect. 1.1. Below, CLUSTER and IMAGE findings are classified into either new findings, confirmation of whistler studies, or further extensions.

Substorm responses of the electric fields are extensively studied using IMAGE data. Ripples or indentations at the plasmapause propagate from nightside toward dusk/dawn MLT, while ground whistler measurements revealed electric field variation first in the westward direction and often subsequently in the eastward direction. Perhaps, both IMAGE and whistler

receivers detect similar phenomena. If this is true, IMAGE has advanced and changed our view on spatial and temporal evolution of substorms from global images.

When the IMF is northward corresponding to small geomagnetic activity, CLUSTER observed electric fields, which are thought to be caused by the ionospheric dynamo effect. This is confirmation of the whistler results. Subcorotation found by IMAGE (Burch et al. 2004) is also interpreted to be caused by the ionospheric dynamo during moderate geomagnetic activity. Further comparison could be made between different instruments at similar geomagnetic activity in future analyses.

The SAPS (or SAID) phenomenon is investigated by IMAGE and CLUSTER. The whistler measurements also reported this large electric field in the duskside. The contribution by IMAGE and CLUSTER studies with combination of DMSP data is to understand the PBL, SED, and M–I coupling through simultaneous measurements at both regions and with various types of instruments. The relationship between the formation of the westward edge of the convection plume and SAPS is new, as well as the apparent close connection between the ionospheric SED and the plume.

Further CLUSTER and IMAGE achievements are to find correlation with IMF and plasmaspheric wind and to extend understanding of undershielding and overshielding effects.

Although various features of plasmaspheric fields are revealed as discussed in this review, further analyses are required to better understand the phenomena. We can identify the following questions guide future directions of research.

1. What are the observational implications on how the electric field is related to other important dynamics in the magnetosphere, such as ring current and radiation belt? The ring current and the electric field are expected to affect each other according to Vasyliunas (1970). What types of mechanisms exactly go on? Quantitative understanding is valuable for this purpose. Radiation belt particles are also related to the background electric fields. For example, the location of the plasmasphere is a parameter that controls the growth rate of ULF and VLF waves and is related to acceleration/deceleration of these particles. Behaviors of trapped particles dependent on the background magnetic field strength suggested by Lemaire et al. (2005) could be investigated in terms of this context as well.
2. What is the physical mechanism, which differentiates between prolonged SAPS and spatially-limited and impulsive SAID? It is necessary to use detailed observations at the ionosphere and magnetosphere combined with modeling studies. Observation of spatial/temporal variability of SAPS with spatially distributed CLUSTER-type instruments would be useful. The dynamics of the PBL would be thus interpreted more consistently.
3. It is important to derive time-dependent inner magnetospheric disturbance electric field models. In particular, the model should be dependent on substorm/storm phases. The developed model is useful to understand the dynamics of the plasmasphere and to compare with simulation results. As these substorms/storms are originally caused by interplanetary parameter changes, this problem is related to the investigation of the Sun–Earth connection. This work complements space weather efforts to achieve better forecasting capabilities.
4. The AC component of the electric field (inductive field and ULF waves) is as large as the DC component. What is the occurrence and distribution of the AC component? Quantitative understanding of ring current acceleration by the AC component and its effect on plasma distribution is a future topic.
5. Field measurements are available at various altitudes from the ground toward the magnetosphere. Combined data analysis between CLUSTER, IMAGE, DMSP, radars, and whistler measurements would lead to a more comprehensive view of the plasmasphere.

Acknowledgements H. Matsui and P. A. Puhl-Quinn acknowledge the support by NASA through grants NNG05GG50G and NNX07AI03G. J. De Keyser and F. Darrouzet acknowledge the support by the Belgian Federal Science Policy Office (BELSPO) through the ESA/PRODEX CLUSTER project (contract 13127/98/NL/VJ (IC)). This paper is an outcome of the workshop "The Earth's plasmasphere: A CLUSTER, IMAGE, and modeling perspective", organized by the Belgian Institute for Space Aeronomy in Brussels in September 2007.

References

P.C. Anderson, W.B. Hanson, R.A. Heelis, J.D. Craven, D.N. Baker, L.A. Frank, A proposed production model of rapid subauroral ion drifts and their relationship to substorm evolution. J. Geophys. Res. **98**(A4), 6069–6078 (1993)

P.C. Anderson, D.L. Carpenter, K. Tsuruda, T. Mukai, F.J. Rich, Multisatellite observations of rapid subauroral ion drifts (SAID). J. Geophys. Res. **106**(A12), 29585–29599 (2001)

H.F. Balmforth, M.A. Clilverd, A.J. Smith, A case study of storm commencement and recovery plasmaspheric electric fields near $L = 2.5$ at equinox. Ann. Geophys. **12**(7), 625–635 (1994)

A. Balogh, C.M. Carr, M.H. Acuña, M.W. Dunlop, T.J. Beek, P. Brown, K.H. Fornaçon, E. Georgescu, K.H. Glassmeier, J. Harris, G. Musmann, T. Oddy, K. Schwingenschuh, The Cluster magnetic field investigation: overview of in-flight performance and initial results. Ann. Geophys. **19**(10–12), 1207–1217 (2001)

W. Baumjohann, G. Haerendel, Magnetospheric convection observed between 0600 and 2100 LT: Solar wind and IMF dependence. J. Geophys. Res. **90**(A7), 6370–6378 (1985)

W. Baumjohann, G. Haerendel, F. Melzner, Magnetospheric convection observed between 0600 and 2100 LT: Variations with *Kp*. J. Geophys. Res. **90**(A1), 393–398 (1985)

W. Baumjohann, R. Nakamura, G. Haerendel, Dayside equatorial-plane convection and IMF sector structure. J. Geophys. Res. **91**(A4), 4557–4560 (1986)

L.P. Block, D.L. Carpenter, Derivation of magnetospheric electric fields from whistler data in a dynamic geomagnetic field. J. Geophys. Res. **79**(19), 2783–2789 (1974)

N.M. Brice, Bulk motion of the magnetosphere. J. Geophys. Res. **72**(21), 5193–5211 (1967)

J.L. Burch, IMAGE mission overview. Space Sci. Rev. **91**(1–2), 1–14 (2000)

J.L. Burch, J. Goldstein, B.R. Sandel, Cause of plasmasphere corotation lag. Geophys. Res. Lett. **31**, L05802 (2004)

D.L. Carpenter, Whistler studies of the plasmapause in the magnetosphere, 1. Temporal variations in the position of the knee and some evidence on plasma motions near the knee. J. Geophys. Res. **71**(3), 693–709 (1966)

D.L. Carpenter, Whistler evidence of the dynamic behavior of the duskside bulge in the plasmasphere. J. Geophys. Res. **75**(19), 3837–3847 (1970)

D.L. Carpenter, J. Lemaire, The plasmasphere boundary layer. Ann. Geophys. **22**(12), 4291–4298 (2004)

D.L. Carpenter, N.T. Seely, Cross-L plasma drifts in the outer plasmasphere: Quiet time patterns and some substorm effects. J. Geophys. Res. **81**(16), 2728–2736 (1976)

D.L. Carpenter, K. Stone, Direct detection by a whistler method of the magnetospheric electric field associated with a polar substorm. Planet. Space Sci. **15**(2), 395–397 (1967)

D.L. Carpenter, C.G. Park, T.R. Miller, A model of substorm electric fields in the plasmasphere based on whistler data. J. Geophys. Res. **84**(A11), 6559–6563 (1979)

D.L. Carpenter, K. Stone, J.C. Siren, T.L. Crystal, Magnetospheric electric fields deduced from drifting whistler paths. J. Geophys. Res. **77**(16), 2819–2834 (1972)

S.W.H. Cowley, Magnetospheric asymmetries associated with the Y-component of the IMF. Planet. Space Sci. **29**(1), 79–96 (1981)

N.U. Crooker, F.J. Rich, Lobe cell convection as a summer phenomenon. J. Geophys. Res. **98**(A8), 13403–13407 (1993)

P. C:son Brandt, S. Ohtani, D.G. Mitchell, M.C. Fok, E.C. Roelof, R. Demajistre, Global ENA observations of the storm mainphase ring current: implications for skewed electric fields in the inner magnetosphere. Geophys. Res. Lett. **29**(20), 1954 (2002)

F. Darrouzet, J. De Keyser, P.M.E. Décréau, J.F. Lemaire, M.W. Dunlop, Spatial gradients in the plasmasphere from Cluster. Geophys. Res. Lett. **33**, L08105 (2006)

F. Darrouzet, D.L. Gallagher, N. André, D.L. Carpenter, I. Dandouras, P.M.E. Décréau, J. De Keyser, R.E. Denton, J.C. Foster, J. Goldstein, M.B. Moldwin, B.W. Reinisch, B.R. Sandel, J. Tu, Plasmaspheric density structures and dynamics: Properties observed by the CLUSTER and IMAGE missions. Space Sci. Rev. (2008). This issue

J. De Keyser, Formation and evolution of subauroral ion drifts in the course of a substorm. J. Geophys. Res. **104**(A6), 12339–12349 (1999)
J. De Keyser, M. Roth, J. Lemaire, The magnetospheric driver of subauroral ion drifts. Geophys. Res. Lett. **25**(10), 1625–1628 (1998)
J. De Keyser, F. Darrouzet, M.W. Dunlop, P.M.E. Décréau, Least-squares gradient calculation from multi-point observations of scalar and vector fields: methodology and applications with Cluster in the plasmasphere. Ann. Geophys. **25**(4), 971–987 (2007)
J. De Keyser, D.L. Carpenter, F. Darrouzet, D.L. Gallagher, J. Tu, CLUSTER and IMAGE: New ways to study the Earth's plasmasphere. Space Sci. Rev. (2008). This issue
O. de la Beaujardiere, D. Alcayde, J. Fontanari, C. Leger, Seasonal dependence of high-latitude electric fields. J. Geophys. Res. **96**(A4), 5723–5735 (1991)
P.M.E. Décréau, P. Fergeau, V. Krasnosels'kikh, E. Le Guirriec, M. Lévêque, P. Martin, O. Randriamboarison, J.L. Rauch, F.X. Sené, H.C. Séran, J.G. Trotignon, P. Canu, N. Cornilleau, H. de Féraudy, H. Alleyne, K. Yearby, P.B. Mögensen, G. Gustafsson, M. André, D.A. Gurnett, F. Darrouzet, J. Lemaire, C.C. Harvey, P. Travnicek, Early results from the Whisper instrument on Cluster: an overview. Ann. Geophys. **19**(10–12), 1241–1258 (2001)
M.W. Dunlop, A. Balogh, Q.Q. Shi, Z. Pu, C. Vallat, P. Robert, S. Haaland, C. Shen, J.A. Davies, K.H. Glassmeier, P. Cargill, F. Darrouzet, A. Roux, The Curlometer and other gradient measurements with Cluster. Proceedings of the Cluster and Double Star Symposium, 5th Anniversary of Cluster in Space **ESA SP-598** (2006)
A.I. Eriksson, M. André, B. Klecker, H. Laakso, P.-A. Lindqvist, F. Mozer, G. Paschmann, A. Pedersen, J. Quinn, R. Torbert, K. Torkar, H. Vaith, Electric field measurements on Cluster: comparing the double-probe and electron drift techniques. Ann. Geophys. **24**(1), 275–289 (2006)
C.P. Escoubet, C.T. Russell, R. Schmidt (eds.), *The Cluster and Phoenix Missions* (Kluwer, Dordrecht, 1997), p. 658
B.G. Fejer, L. Scherliess, Time dependent response of equatorial ionospheric electric fields to magnetospheric disturbances. Geophys. Res., Lett. **22**(7), 851–854 (1995)
B.G. Fejer, R.W. Spiro, R.A. Wolf, J.C. Foster, Latitudinal variation of perturbation electric fields during magnetically disturbed periods—1986 Sundial observations and model results. Ann. Geophys. **8**(6), 441–454 (1990)
S. Figueiredo, T. Karlsson, G.T. Marklund, Investigation of subauroral ion drifts and related field-aligned currents and ionospheric Pedersen conductivity distribution. Ann. Geophys. **22**(3), 923–934 (2004)
J.C. Foster, Storm time plasma transport at middle and high latitudes. J. Geophys. Res. **98**(A2), 1675–1689 (1993)
J.C. Foster, W.J. Burke, SAPS: A new categorization for sub-auroral electric fields. Eos Trans. AGU **83**(36), 393 (2002)
J.C. Foster, H.B. Vo, Average characteristics and activity dependence of the subauroral polarization stream. J. Geophys. Res. **107**(A12), 1475 (2002)
J.C. Foster, J.M. Holt, R.G. Musgrove, D.S. Evans, Ionospheric convection associated with discrete levels of particle precipitation. Geophys. Res. Lett. **13**(7), 656–659 (1986)
J.C. Foster, P.J. Erickson, A.J. Coster, J. Goldstein, F.J. Rich, Ionospheric signatures of plasmaspheric tails. Geophys. Res. Lett. **29**(13), 1623 (2002)
J.C. Foster, W. Rideout, B. Sandel, W.T. Forrester, F.J. Rich, On the relationship of SAPS to storm-enhanced density. J. Atmos. Sol.-Terr. Phys. **69**(3), 303–313 (2007)
D.L. Gallagher, M.L. Adrian, Two-dimensional drift velocities from the IMAGE EUV plasmaspheric imager. J. Atmos. Sol.-Terr. Phys. **69**(3), 341–350 (2007)
Y.I. Galperin, V.N. Ponomarev, A.G. Zosimova, Plasma convection in the polar ionosphere. Ann. Geophys. **30**(1), 1–7 (1974)
J. Goldstein, Plasmasphere response: Tutorial and review of recent imaging results. Space Sci. Rev. **124**(1–4), 203–216 (2006)
J. Goldstein, B.R. Sandel, The global pattern of evolution of plasmaspheric drainage plumes, in *Inner Magnetosphere Interactions: New Perspectives from Imaging*, ed. by J.L. Burch, M. Schulz, H. Spence. Geophysical Monograph Series, vol. 159 (American Geophysical Union, Washington, 2005), pp. 1–22
J. Goldstein, R.W. Spiro, P.H. Reiff, R.A. Wolf, B.R. Sandel, J.W. Freeman, R.L. Lambour, IMF-driven overshielding electric field and the origin of the plasmaspheric shoulder of May 24, 2000. Geophys. Res. Lett. **29**(16), 1819 (2002)
J. Goldstein, B.R. Sandel, W.T. Forrester, P.H. Reiff, IMF-driven plasmasphere erosion of 10 July 2000. Geophys. Res. Lett. **30**(3), 1146 (2003a)
J. Goldstein, B.R. Sandel, M.R. Hairston, P.H. Reiff, Control of plasmaspheric dynamics by both convection and sub-auroral polarization stream. Geophys. Res. Lett. **30**(24), 2243 (2003b)

J. Goldstein, R.W. Spiro, B.R. Sandel, R.A. Wolf, S.Y. Su, P.H. Reiff, Overshielding event of 28–29 July 2000. Geophys. Res. Lett. **30**(8), 1421 (2003c)
J. Goldstein, B.R. Sandel, M.R. Hairston, S.B. Mende, Plasmapause undulation of 17 April 2002. Geophys. Res. Lett. **31**, L15801 (2004a)
J. Goldstein, R.A. Wolf, B.R. Sandel, P.H. Reiff, Electric fields deduced from plasmapause motion in IMAGE EUV images. Geophys. Res. Lett. **31**, L01801 (2004b)
J. Goldstein, J.L. Burch, B.R. Sandel, Magnetospheric model of subauroral polarization stream. J. Geophys. Res. **110**, A09222 (2005a)
J. Goldstein, J.L. Burch, B.R. Sandel, S.B. Mende, P. C:son Brandt, M.R. Hairston, Coupled response of the inner magnetosphere and ionosphere on 17 April 2002. J. Geophys. Res. **110**, A03205 (2005b)
J. Goldstein, B.R. Sandel, W.T. Forrester, M.F. Thomsen, M.R. Hairston, Global plasmasphere evolution 22–23 April 2001. J. Geophys. Res. **110**, A12218 (2005c)
J. Goldstein, B.R. Sandel, H.U. Frey, S.B. Mende, Multiple plasmapause undulations observed by the IMAGE satellite on 20 March 2001. J. Atmos. Sol.-Terr. Phys. **69**(3), 322–333 (2007)
C.A. Gonzales, M.C. Kelley, D.L. Carpenter, T.R. Miller, R.H. Wand, Simultaneous measurements of ionospheric and magnetospheric electric fields in the outer plasmasphere. Geophys. Res. Lett. **7**(7), 517–520 (1980)
G. Gustafsson, M. André, T. Carozzi, A.I. Eriksson, C.G. Fälthammar, R. Grard, G. Holmgren, J.A. Holtet, N. Ivchenko, T. Karlsson, Y. Khotyaintsev, S. Klimov, H. Laakso, P.-A. Lindqvist, B. Lybekk, G. Marklund, F. Mozer, K. Mursula, A. Pedersen, B. Popielawska, S. Savin, K. Stasiewicz, P. Tanskanen, A. Vaivads, J.E. Wahlund, First results of electric field and density observations by Cluster EFW based on initial months of observations. Ann. Geophys. **19**(10–12), 1219–1240 (2001)
C.C. Harvey, Spatial gradients and the volumetric tensor, in *Analysis Methods for Multi-Spacecraft Data*, ed. by G. Paschmann, P.W. Daly. ISSI SR-001 (ESA Publications Division, Noordwijk, 1998), pp. 307–322
R.A. Heelis, W.R. Coley, East–West ion drifts at mid-latitudes observed by Dynamics Explorer 2. J. Geophys. Res. **97**(A12), 19461–19469 (1992)
R.A. Helliwell, *Whistlers and Associated Ionospheric Phenomena* (Stanford University Press, Stanford, 1965), p. 349
J.P. Heppner, N.C. Maynard, Empirical high-latitude electric field models. J. Geophys. Res. **92**(A5), 4467–4489 (1987)
C.S. Huang, G.D. Reeves, G. Le, K. Yumoto, Are sawtooth oscillations of energetic plasma particle fluxes caused by periodic substorms or driven by solar wind pressure enhancements? J. Geophys. Res. **110**, A07207 (2005)
C. Huang, S. Sazykin, R. Spiro, J. Goldstein, G. Crowley, J.M. Ruohoniemi, Storm-time penetration electric fields and their effects. Eos Trans. AGU **87**(13), 131 (2006)
R.K. Jaggi, R.A. Wolf, Self-consistent calculation of the motion of a sheet of ions in the magnetosphere. J. Geophys. Res. **78**(16), 2852–2866 (1973)
T. Karlsson, G.T. Marklund, L.G. Blomberg, A. Mälkki, Subauroral electric fields observed by the Freja satellite: A statistical study. J. Geophys. Res. **103**(A3), 4327–4341 (1998)
H. Khan, S.W.H. Cowley, Observations of the response time of high-latitude ionospheric convection to variations in the interplanetary magnetic field using EISCAT and IMP-8 data. Ann. Geophys. **17**(10), 1306–1335 (1999)
B.A. Larsen, D.M. Klumpar, C. Gurgiolo, Correlation between plasmapause position and solar wind parameters. J. Atmos. Sol.-Terr. Phys. **69**(3), 334–340 (2007)
J.F. Lemaire, K.I. Gringauz, *The Earth's Plasmasphere* (Cambridge University Press, New York, 1998), p. 372
J.F. Lemaire, S.G. Batteux, I.N. Slypen, The influence of a southward and northward turning of the interplanetary magnetic field on the geomagnetic cut-off of cosmic rays, on the mirror points positions of geomagnetically trapped particles, and on their rate of precipitations in the atmosphere. J. Atmos. Sol.-Terr. Phys. **67**(7), 719–727 (2005)
H. Matsui, J.M. Quinn, R.B. Torbert, V.K. Jordanova, W. Baumjohann, P.A. Puhl-Quinn, G. Paschmann, Electric field measurements in the inner magnetosphere by Cluster EDI. J. Geophys. Res. **108**(A9), 1352 (2003)
H. Matsui, V.K. Jordanova, J.M. Quinn, R.B. Torbert, G. Paschmann, Derivation of electric potential patterns in the inner magnetosphere from Cluster EDI data: Initial results. J. Geophys. Res. **109**, A10202 (2004)
H. Matsui, J.M. Quinn, R.B. Torbert, V.K. Jordanova, P.A. Puhl-Quinn, G. Paschmann, IMF $\boldsymbol{B_y}$ and seasonal dependences of the electric field in the inner magnetosphere. Ann. Geophys. **23**(7), 2671–2678 (2005)
H. Matsui, P.A. Puhl-Quinn, V.K. Jordanova, Y. Khotyaintsev, P.-A. Lindqvist, R.B. Torbert, Derivation of inner magnetospheric electric field (UNH-IMEF) model using Cluster data set. Ann. Geophys. **26**(9), 2887–2898 (2008)

N.C. Maynard, A.J. Chen, Isolated cold plasma regions: observations and their relation to possible production mechanisms. J. Geophys. Res. **80**(7), 1009–1013 (1975)

N.C. Maynard, T.L. Aggson, J.P. Heppner, The plasmaspheric electric field as measured by ISEE 1. J. Geophys. Res. **88**(A5), 3991–4003 (1983)

D.J. McComas, S.J. Bame, P. Barker, W.C. Feldman, J.L. Phillips, P. Riley, J.W. Griffee, Solar Wind Electron Proton Alpha Monitor (SWEPAM) for the Advanced Composition Explorer. Space Sci. Rev. **86**(1–4), 563–612 (1998)

C.E. McIlwain, Substorm injection boundaries, in *Magnetospheric Physics*, ed. by B.M. McCormac (Reidel, Dordrecht, 1974), pp. 143–154

F.A. McNeill, Frequency shifts on whistler mode signals from a stabilized VLF transmitter. Radio Sci. **2**, 589–594 (1967)

E.V. Mishin, P.A. Puhl-Quinn, SAID: plasmaspheric short circuit of substorm injections. Geophys. Res. Lett. **34**, L24101 (2007)

A. Nishida, Formation of plasmapause, or magnetospheric plasma knee, by the combined action of magnetospheric convection and plasma escape from the tail. J. Geophys. Res. **71**(23), 5669–5679 (1966)

R.W. Nopper, R.L. Carovillano, Polar-equatorial coupling during magnetically active periods. Geophys. Res. Lett. **5**(8), 699–702 (1978)

G. Paschmann, J.M. Quinn, R.B. Torbert, H. Vaith, C.E. McIlwain, G. Haerendel, O.H. Bauer, T. Bauer, W. Baumjohann, W. Fillius, M. Förster, S. Frey, E. Georgescu, S.S. Kerr, C.A. Kletzing, H. Matsui, P. Puhl-Quinn, E.C. Whipple, The electron drift instrument on Cluster: overview of first results. Ann. Geophys. **19**(10–12), 1273–1288 (2001)

V. Pierrard, J. Goldstein, N. André, V.K. Jordanova, G.A. Kotova, J.F. Lemaire, M.W. Liemohn, H. Matsui, Recent progress in physics-based models of the plasmasphere. Space Sci. Rev. (2008). This issue

P.A. Puhl-Quinn, H. Matsui, E. Mishin, C. Mouikis, L. Kistler, Y. Khotyaintsev, P.M.E. Décréau, E. Lucek, Cluster and DMSP observations of SAID electric fields. J. Geophys. Res. **112**, A05219 (2007)

P.A. Puhl-Quinn, H. Matsui, V.K. Jordanova, Y. Khotyaintsev, P.-A. Lindqvist, An effort to derive an empirically based, inner-magnetospheric electric field model: Merging Cluster EDI and EFW data. J. Atmos. Sol.-Terr. Phys. **70**(2–4), 564–573 (2008)

J.M. Quinn, G. Paschmann, N. Sckopke, V.K. Jordanova, H. Vaith, O.H. Bauer, W. Baumjohann, W. Fillius, G. Haerendel, S.S. Kerr, C.A. Kletzing, K. Lynch, C.E. McIlwain, R.B. Torbert, E.C. Whipple, EDI convection measurements at 5–6 R_E in the post-midnight region. Ann. Geophys. **17**(12), 1503–1512 (1999)

J.M. Quinn, G. Paschmann, R.B. Torbert, H. Vaith, C.E. McIlwain, G. Haerendel, O. Bauer, T.M. Bauer, W. Baumjohann, W. Fillius, M. Foerster, S. Frey, E. Georgescu, S.S. Kerr, C.A. Kletzing, H. Matsui, P. Puhl-Quinn, E.C. Whipple, Cluster EDI convection measurements across the high-latitude plasma sheet boundary at midnight. Ann. Geophys. **19**(10–12), 1669–1681 (2001)

B.W. Reinisch, M.B. Moldwin, R.E. Denton, D.L. Gallagher, H. Matsui, V. Pierrard, J. Tu, Augmented empirical models of plasmaspheric density and electric field using IMAGE and CLUSTER data. Space Sci. Rev. (2008). This issue

H. Rème, C. Aoustin, J.M. Bosqued, I. Dandouras, B. Lavraud, J.A. Sauvaud, A. Barthe, J. Bouyssou, Th. Camus, O. Coeur-Joly, A. Cros, J. Cuvilo, F. Ducay, Y. Garbarowitz, J.L. Médale, E. Penou, H. Perrier, D. Romefort, J. Rouzaud, C. Vallat, D. Alcaydé, C. Jacquey, C. Mazelle, C. d'Uston, E. Möbius, L.M. Kistler, K. Crocker, M. Granoff, C. Mouikis, M. Popecki, M. Vosbury, B. Klecker, D. Hovestadt, H. Kucharek, E. Kuenneth, G. Paschmann, M. Scholer, N. Sckopke, E. Seidenschwang, C.W. Carlson, D.W. Curtis, C. Ingraham, R.P. Lin, J.P. McFadden, G.K. Parks, T. Phan, V. Formisano, E. Amata, M.B. Bavassano-Cattaneo, P. Baldetti, R. Bruno, G. Chionchio, A. Di Lellis, M.F. Marcucci, G. Pallocchia, A. Korth, P.W. Daly, B. Graeve, H. Rosenbauer, V. Vasyliunas, M. McCarthy, M. Wilber, L. Eliasson, R. Lundin, S. Olsen, E.G. Shelley, S. Fuselier, A.G. Ghielmetti, W. Lennartsson, C.P. Escoubet, H. Balsiger, R. Friedel, J.-B. Cao, R.A. Kovrazhkin, I. Papamastorakis, R. Pellat, J. Scudder, B. Sonnerup, First multi-spacecraft ion measurements in and near the Earth's magnetosphere with the identical Cluster Ion Spectrometry (CIS) experiment. Ann. Geophys. **19**(10–12), 1303–1354 (2001)

F.J. Rich, W.J. Burke, M.C. Kelley, M. Smiddy, Observations of field-aligned currents in association with strong convection electric fields at subauroral latitudes. J. Geophys. Res. **85**(A5), 2335–2340 (1980)

A.J. Ridley, G. Lu, C.R. Clauer, V.O. Papitashvili, A statistical study of the ionospheric convection response to changing interplanetary magnetic field conditions using the assimilative mapping of ionospheric electrodynamics technique. J. Geophys. Res. **103**(A3), 4023–4039 (1998)

D.E. Rowland, J.R. Wygant, Dependence of the large-scale, inner magnetospheric electric field on geomagnetic activity. J. Geophys. Res. **103**(A7), 14959–14964 (1998)

B.R. Sandel, R.A. King, W.T. Forrester, D.L. Gallagher, A.L. Broadfoot, C.C. Curtis, Initial results from the IMAGE Extreme Ultraviolet imager. Geophys. Res. Lett. **28**(8), 1439–1442 (2001)

J.M. Saxton, A.J. Smith, Quiet time plasmaspheric electric fields and plasmasphere–ionosphere coupling fluxes at $L = 2.5$. Planet. Space Sci. **37**(3), 283–293 (1989)

S. Sazykin, R.W. Spiro, R.A. Wolf, F.R. Toffoletto, N. Tsyganenko, J. Goldstein, M.R. Hairston, Modeling inner magnetospheric electric fields: latest self-consistent results, in *The Inner Magnetosphere: Physics and Modeling*, ed. by T.I. Pulkkinen, N.A. Tsyganenko, R.H.W. Friedel. Geophysical Monograph Series, vol. 155 (American Geophysical Union, Washington, 2005), pp. 263–269

L. Scherliess, B.G. Fejer, Storm time dependence of equatorial disturbance dynamo zonal electric fields. J. Geophys. Res. **102**(A11), 24037–24046 (1997)

R.W. Schunk, P.M. Banks, W.J.Raitt, Effects of electric fields and other processes upon the nighttime high-latitude F layer. J. Geophys. Res. **81**(19), 3271–3282 (1976)

M. Smiddy, M.C. Kelley, W. Burke, F. Rich, R. Sagalyn, B. Shuman, R. Hays, S. Lai, Intense poleward-directed electric fields near the ionospheric projection of the plasmapause. Geophys. Res. Lett. **4**(11), 543–546 (1977)

A.J. Smith, K.H. Yearby, K. Bullough, J.M. Saxton, H.J. Strangeways, N.R. Thomson, Whistler mode signals from VLF transmitters observed at Faraday, Antarctica. Mem. Nat. Inst. Polar Res. **48**, 183–195 (1987)

C.W. Smith, J. L'Heureux, N.F. Ness, M.H. Acuña, L.F. Burlaga, J. Scheifele, The ACE magnetic fields experiment. Space Sci. Rev. **86**(1–4), 613–632 (1998)

R.L. Smith, Propagation Characteristics of whistlers trapped in field-aligned columns of enhanced ionization. J. Geophys. Res. **66**(11), 3699–3707 (1961)

M. Spasojević, J. Goldstein, D.L. Carpenter, U.S. Inan, B.R. Sandel, M.B. Moldwin, B.W. Reinisch, Global response of the plasmasphere to a geomagnetic disturbance. J. Geophys. Res. **108**(A9), 1340 (2003)

R.W. Spiro, R.A. Heelis, W.B. Hanson, Rapid subauroral ion drifts observed by Atmospheric Explorer C. Geophys. Res. Lett. **6**(8), 657–660 (1979)

N.R. Thomson, Electric fields from whistler-mode Doppler shifts. Planet. Space Sci. **24**(5), 455–458 (1976)

N.R. Thomson, Whistler mode signals: spectrographic group delays. J. Geophys. Res. **86**(A6), 4795–4802 (1981)

N.A. Tsyganenko, A model of the near magnetosphere with a dawn–dusk asymmetry 1. Mathematical structure. J. Geophys. Res. **107**(A8), 1179 (2002)

N.A. Tsyganenko, D.P. Stern, Modeling the global magnetic field of the large-scale Birkeland current systems. J. Geophys. Res. **101**(A12), 27187–27198 (1996)

C. Vallat, I. Dandouras, M. Dunlop, A. Balogh, E. Lucek, G.K. Parks, M. Wilber, E.C. Roelof, G. Chanteur, H. Rème, First current density measurements in the ring current region using simultaneous multi-spacecraft CLUSTER-FGM data. Ann. Geophys. **23**(5), 1849–1865 (2005)

V.M. Vasyliunas, Mathematical models of magnetospheric convection and its coupling to the ionosphere, in *Particles and Fields in the Magnetosphere*, ed. by B.M. McCormac (Reidel, Dordrecht, 1970), pp. 60–71

R.H. Wand, J.V. Evans, Seasonal and magnetic activity variations of ionospheric electric fields over Millstone Hill. J. Geophys. Res. **86**(A1), 103–118 (1981)

D.R. Weimer, An improved model of ionospheric electric potentials including substorm perturbations and application to the Geospace Environment Modeling November 24, 1996, event. J. Geophys. Res. **106**(A1), 407–416 (2001)

R.A. Wolf, Effects of ionospheric conductivity on convective flow of plasma in the magnetosphere. J. Geophys. Res. **75**(25), 4677–4698 (1970)

R.A. Wolf, S. Sazykin, X. Xing, R.W. Spiro, F.R. Toffoletto, D.L. DeZeeuw, T.I. Gombosi, J. Goldstein, Direct effects of the IMF on the inner magnetosphere, in *Inner Magnetosphere Interactions: New Perspectives from Imaging*, ed. by J.L. Burch, M. Schulz, H. Spence. Geophysical Monograph Series, vol. 159 (American Geophysical Union, Washington, 2005), pp. 127–140

J. Wygant, D. Rowland, H.J. Singer, M. Temerin, F. Mozer, M.K. Hudson, Experimental evidence on the role of the large spatial scale electric field in creating the ring current. J. Geophys. Res. **103**(A12), 29527–29544 (1998)